Translational Stroke Research
https://doi.org/10.1007/s12975-024-01240-1

RESEARCH

GPR39 Agonist TC-G 1008 Promoted Mitochondrial Biogenesis and Improved Antioxidative Capability via CREB/PGC-1α Pathway Following Intracerebral Hemorrhage in Mice

Zhongyi Zhang[1] · Ye Yuan[1] · Xingyu Zhang[1] · Lingui Gu[2] · Yuguang Tang[1] · Yutong Zhao[1] · Jinyu Dai[1] · Yihao Tao[1] · Zongyi Xie[1]

Received: 13 November 2023 / Revised: 11 February 2024 / Accepted: 1 March 2024
© The Author(s), under exclusive licence to Springer Science+Business Media, LLC, part of Springer Nature 2024

Abstract

Mitochondrial dysfunction and excessive reactive oxygen species production due to impaired mitochondrial biogenesis have been proven to exacerbate secondary brain injury after intracerebral hemorrhage (ICH). The G-protein-coupled receptor 39 (GPR39) agonist TC-G 1008 has been shown to exert anti-oxidative stress effect in acute hypoxic brain injury. Herein, our study aimed to investigate the potential effects of TC-G 1008 on neuronal mitochondrial biogenesis and antioxidative stress in a mouse model of ICH and explore the underlying mechanisms. A total of 335 male C57/BL6 mice were used to establish an autologous blood-induced ICH model. Three different dosages of TC-G 1008 were administered via oral gavage at 1 h, 25 h, and 49 h post-ICH. The GPR39 siRNA and cAMP response element-binding protein (CREB) inhibitor 666–15 were administered via intracerebroventricular injection before ICH insult to explore the underlying mechanisms. Neurobehavioral function tests, Western blot, quantitative polymerase chain reaction, immunofluorescence staining, Fluoro-Jade C staining, TUNEL staining, dihydroethidium staining, transmission electron microscopy, and enzyme-linked immunosorbent assay were performed. Expression of endogenous GPR39 gradually increased in a time-dependent manner in the peri-hematoma tissues, peaking between 24 and 72 h after ICH. Treatment with TC-G 1008 significantly attenuated brain edema, hematoma size, neuronal degeneration, and neuronal death, as well as improved neurobehavioral deficits at 72 h after ICH. Moreover, TC-G 1008 upregulated the expression of mitochondrial biogenesis-related molecules, including PGC-1α, NRF1, TFAM, and mitochondrial DNA copy number, associated with antioxidative stress markers, such as Nrf2, HO-1, NQO1, SOD, CAT, and GSH-Px. Furthermore, treatment with TC-G 1008 preserved neuronal mitochondrial function and structure post-ICH. Mechanistically, the protective effects of TC-G 1008 on neuronal mitochondrial biogenesis and antioxidative stress were partially reversed by GPR39 siRNA or 666 -15. Our findings indicated that GPR39 agonist TC-G 1008 promoted mitochondrial biogenesis and improved antioxidative capability after ICH, partly through the CREB/PGC-1α signaling pathway. TC-G 1008 may be a potential therapeutic agent for patients with ICH.

Keywords Intracerebral hemorrhage · Mitochondrial biogenesis · Antioxidative capability · G-protein-coupled receptor 39 · TC-G 1008

Introduction

The mechanism of secondary brain injury (SBI) induced by intracerebral hemorrhage (ICH) is intricate and not yet fully understood [1, 2]. Mitochondrial dysfunction and excessive production of reactive oxygen species (ROS) are considered to be involved in the pathogenesis of SBI after ICH [3, 4]. Therefore, improving mitochondrial dysfunction could be a promising therapeutic approach for ameliorating SBI following ICH [5, 6].

Mitochondrial biogenesis, a multifaceted regulatory process, is crucial for maintaining cellular homeostasis [7]. Mounting evidence indicated that mitochondrial biogenesis plays a central role in enhancing oxidative phosphorylation capacity, alleviating pathological oxidative stress, and improving mitochondrial dysfunction [8]. Specifically, mitochondrial biogenesis governs oxidative phosphorylation to produce adenosine triphosphate (ATP), facilitates mitochondrial DNA (mtDNA) replication, removes damaged mitochondria, and preserves membrane potential and redox balance [9]. It has been established that

Extended author information available on the last page of the article

Published online: 15 March 2024

impaired mitochondrial biogenesis leads to mitochondrial dysfunction and excessive ROS production [10]. Moreover, regulating mitochondrial biogenesis has a protective effect against heart failure and liver injury caused by ischemia–reperfusion, as well as promoting the repair of renal tubular epithelial cells [11–13]. In addition, in a rat model of subarachnoid hemorrhage (SAH), promoting mitochondrial biogenesis could alleviate brain injury by inhibiting neuronal apoptosis [14]. Thus, promoting mitochondrial biogenesis and enhancing antioxidative capability could attenuate SBI after ICH.

G-protein-coupled receptor 39 (GPR39), a prototypical member of the G protein-coupled receptors (GPCRs) family, is expressed in the heart, gastrointestinal tract, and multiple brain regions [15]. GPR39 was involved in various pathological processes, such as promoting wound healing, alleviating symptoms related to inflammatory bowel disease, reducing anxiety-related behaviors, regulating insulin secretion, and influencing the progression of malignant cancers [16–20]. Previous studies have shown that activation of GPR39 exerts neuroprotective effects through anti-apoptotic, anti-inflammatory, and antioxidative pathways [21–23]. On the contrary, GPR39 knockout exacerbated microvascular perfusion and brain injury after ischemic brain injury in mice [24]. Nevertheless, the role of GPR39 in mitochondrial function following ICH remains to be elucidated.

Recently, Mo et al. reported that TC-G 1008, a potent GPR39 agonist, upregulated the expression of intracellular cAMP response element binding protein (CREB) [22]. Previous studies have demonstrated that phosphorylated CREB orchestrates metabolic adaptation by upregulating the expression of peroxisome proliferator-activated receptor gamma coactivator 1-alpha (PGC-1α) [10]. PGC-1α, a key regulator of mitochondrial biogenesis and antioxidative defense, upregulates the expression of genes related to mitochondrial biogenesis, such as nuclear respiratory factors-1 (NRF1) and mitochondrial transcription factor A (TFAM) [8]. Nuclear factor erythroid 2-related factor 2 (Nrf2) is a crucial transcription factor, that regulates the expression of essential genes in the antioxidant system, including heme oxygenase 1 (HO-1) and quinone oxidoreductase 1 (NQO1) [25].

In this study, we hypothesized that GPR39 agonist TC-G 1008 could promote mitochondrial biogenesis and improve antioxidative capability via the CREB/PGC-1α signaling pathway after ICH in mice.

Materials and Methods

Animal

The Animal Center of Chongqing Medical University provided 335 male C57BL/6 mice, 6–8 weeks old and 20-25 g. The mice were kept in a controlled setting with a 22 ± 1 °C temperature and a 12-h light/dark cycle. Their living space contained unlimited fresh food and water. The Chongqing Medical University Animal Ethics Committee approved the study.

Experimental Design

As shown in Fig. 1, the study included five independent experiments conducted to investigate the specific research objectives.

Experiment 1

To examine the time course and cellular localization of endogenous GPR39 expression after ICH. Peri-hematoma tissue in the ipsilateral basal ganglia was analyzed by Western blot and double immunofluorescence staining. Mice were randomly divided into 6 groups: Sham ($n = 10$ mice/group), ICH-6 h ($n = 6$ mice/group), ICH-12 h ($n = 6$ mice/group), ICH-24 h ($n = 10$ mice/group), ICH-72 h ($n = 6$ mice/group), ICH-7 day ($n = 6$ mice/group).

Experiment 2

To assess the role of endogenous GPR39 in brain injury after ICH. GPR39 siRNA mixture or Scramble siRNA was delivered by intracerebroventricular injection 48 h before ICH induction. Neurobehavioral function tests and Western blot were performed 72 h after ICH. Mice were randomly divided into 4 groups: Naïve + Scramble siRNA ($n = 6$ mice/group), Naïve + GPR39 siRNA ($n = 6$ mice/group), ICH + Scramble siRNA ($n = 6$ mice/group), ICH + GPR39 siRNA ($n = 6$ mice/group).

Experiment 3

To evaluate the effect of GPR39 agonist TC-G 1008 on brain injury in mice after ICH. Three different dosages of TC-G1008 (8, 24, 72 mg/kg, HY-103007, MCE, Shanghai, China), a specific GPR39 agonist, were administered via oral gavage at three different time points, 1 h, 25 h, and 49 h after the induction of the ICH model. Neurobehavioral function tests were measured at 24 h and 72 h after ICH to evaluate the therapeutic effect. Brain water content and hematoma size were measured at 72 h. Mice were randomized divided into 5 groups: Sham ($n = 6$ mice/group), ICH + Vehicle ($n = 6$ mice/group), ICH + TC-G 1008 (8 mg/kg) ($n = 6$ mice/group), ICH + TC-G 1008 (24 mg/kg) ($n = 6$ mice/group), ICH + TC-G 1008 (72 mg/kg) ($n = 6$ mice/group).

Experiment 4

To investigate the effects of TC-G 1008 on mitochondrial biogenesis and oxidative stress after ICH in mice. GPR39

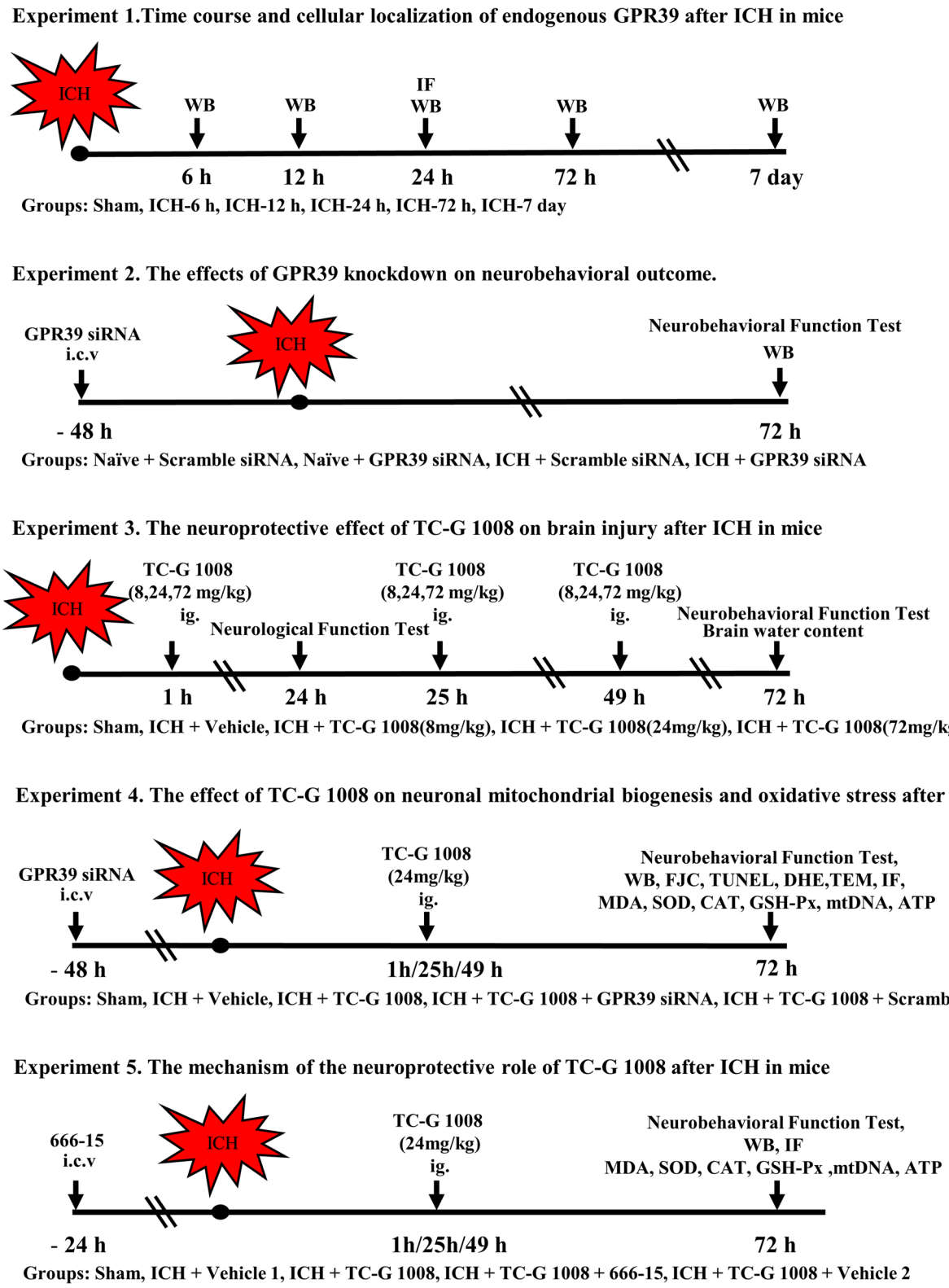

Fig. 1 Experimental design and animal groups. ATP, adenosine triphosphatase; CAT, catalase; DHE, dihydroethidium staining; FJC, Fluoro-Jade C staining; GSH-Px, glutathione peroxidase; i.c.v., intracerebroventricular; ig., gavage; ICH, intracerebral hemorrhage; IF, immunofluorescence staining; mtDNA, mitochondrial DNA; MDA, malondialdehyde; TC-G 1008, GPR39 agonist; TEM, transmission electron microscopy; TUNEL, TdT-mediated dUTP Nick-End Labeling; WB, Western blotting; SOD, superoxide dismutase; 666–15, CREB inhibitor

siRNA was delivered by intracerebroventricular injection 48 h before ICH induction. Western blot, Fluoro-Jade C staining, TUNEL staining, DHE staining, TEM, IF, q-PCR, and ELISA were performed 72 h after ICH. Mice were randomly divided into 5 groups: Sham ($n = 24$ mice/group), ICH + Vehicle ($n = 24$ mice/group), ICH + TC-G 1008 ($n = 24$ mice/group), ICH + TC-G 1008 + GPR39 siRNA ($n = 24$ mice/group), ICH + TC-G 1008 + Scramble siRNA ($n = 24$ mice/group).

Experiment 5

To investigate the underlying mechanism of the neuroprotective role of TC-G 1008 on mitochondrial biogenesis and antioxidative capability after ICH, a specific CREB inhibitor, 666–15, (10 mg/kg, HY-101120, MCE, Shanghai, China), was administered via intracerebroventricular injection at 24 h prior to ICH induction. Neurobehavioral function tests, western blot, IF, q-PCR, and ELISA were performed 72 h after ICH. Mice were randomly divided into 5 groups: Sham ($n = 16$ mice/group), ICH + Vehicle 1 ($n = 16$ mice/group), ICH + TC-G 1008 ($n = 16$ mice/group), ICH + TC-G 1008 + 666–15 ($n = 16$ mice/group), ICH + TC-G 1008 + Vehicle 2 ($n = 16$ mice/group).

ICH Model

Skilled and sophisticated experimenters conducted animal surgical procedures with the aim of minimizing pain and distress during the operation. The autologous blood was used to establish an ICH model, following a method that had been previously outlined in the literature [26]. Following the administration of 1% pentobarbital anesthesia at a dose of 50 mg/kg via intraperitoneal injection, the mice were positioned in a prone orientation and securely affixed within a stereotaxic apparatus. Subsequent to depilation and aseptic skin preparation, a surgical skin flap was meticulously crafted to expose the calvaria. Thereafter, a precise cranial perforation was established at a site positioned 2 mm to the right of the bregma. Subsequently, a controlled infusion of 30 ml of autologous blood, devoid of anticoagulants, obtained from the central tail artery was carefully administered into the basal ganglion at specific stereotaxic coordinates: 0.2 mm anterior, 2.3 mm lateral to the right of the bregma, and a depth of 3.5 mm. To minimize the risk of retrograde blood flow, the needle was intentionally retained in place for a duration of 10 min following the conclusion of the blood injection. Finally, the needle was removed, and the skin was sutured. Mice with unsuccessful ICH models were excluded from the study, and all surgical procedures were conducted with strict adherence to the principle of sterility.

Intracerebroventricular Injection

Intracerebroventricular injections were carried out following the previously described method [27]. Following profound anesthesia, the mice were positioned within a stereotaxic device. A cranial burr hole was created on the skull, and a needle was carefully inserted into the right lateral ventricle, with precise coordinates relative to bregma: 0.3 mm posterior, 1.0 mm lateral, and 2.3 mm deep. Subsequently, the drugs were administered at a controlled rate of 200 nl/min using an infusion pump. Upon completion of the injection, the needle was maintained in its position for an additional 10 min to prevent any potential leakage. It was then gradually withdrawn over a 5-min interval. GPR39 siRNA (GenePharma, Shanghai, China, sense 5′-GCG CUA CAU UGC CAU UUG UTT-3′, antisense 5′-ACA AAU GGC AAU GUA GCG CTT-3′) and Scramble siRNA (GenePharma, Shanghai, China, sense 5′-UUC UCC GAA CGU ACG UTT-3′, antisense 5′-ACG UGA CAC GUU CGG AGA ATT-3′) were dissolved in sterile water treated with diethylpyroearbonate (DPEC) and certified RNase-free. The GPR39 siRNA mixture or scramble siRNA (100 pmol/2 μl) was administered into the ipsilateral ventricle. The heating pad was used to maintain body temperature during both surgical intervention and postoperative recovery.

Neurobehavioral Function Tests

The modified Garcia test, forelimb placement test, and corner turn test were performed by a blinded investigator to assess short-term neurobehavior functions. The modified Garcia test includes assessments for spontaneous activity, axial sensation, vibrissae touch, limb symmetry, lateral turning, forelimb walking, and climbing. Each subtest is assessed using a scoring scale that spans from 0 to 3 or 1 to 3, and the overall score is calculated by adding up the scores across all seven sections. A greater overall score indicates improved neurological functioning. For the forelimb placement test, the experimenter delicately lifted the mouse's body, allowing its forelimb to dangle, and subsequently brushed its left vibrissae against the edge of a countertop. After conducting a series of 10 trials, the frequency at which the mouse positioned its left forelimb on the edge of the countertop was determined. For the corner turn test, the mice were allowed to exit freely from a 30-degree corner to the left or right. A total of ten trials were conducted, with an interval of at least 30 s between each trial. Subsequently, the percentage of right turns out of these ten trials was calculated.

Brain Water Content

To quantify brain edema, brain water content was evaluated 72 h post-ICH by an investigator blinded to the conditions, adhering to a previously documented procedure [28]. The mice were subjected to decapitation while in a state of profound anesthesia, following which their brains were expeditiously removed. The brain was divided into five distinct parts, including the ipsilateral and contralateral basal

ganglia, the ipsilateral and contralateral cortex, and the cerebellum. The cerebellum serves as an internal reference. Each section was promptly measured using an electronic analytical balance to determine the weight when wet. Subsequently, the samples were subjected to a drying process at 100 °C for a duration of 72 h in order to obtain the weight when dry. The percentage of water content in the brain was then calculated using the following formula: brain water content (%) = [(wet weight—dry weight)/wet weight] × 100%.

Preparation of Paraffin-embedded Sections

Paraffin-embedded sections were prepared using a previously outlined protocol with slight adjustments [29]. The mice were deeply anesthetized and underwent transcardial perfusion with 20 ml of ice-cold PBS, followed by a solution containing 4% paraformaldehyde. Immediately after, the entire brain was extracted and placed in a 4% paraformaldehyde solution at a temperature of 4 °C for 48 h. Subsequently, the brain samples were dehydrated using different concentrations of ethanol, cleared with xylene, and finally embedded in paraffin. The embedded samples were then sliced into coronal sections measuring approximately 8 μm thick using a cryostat (CM1860, Leica Microsystems, Germany). Sections ranging from -0.30 to + 0.70 mm relative to the anterior aspect of the gyrus were chosen for further experimentation and analysis purposes. These selected sections underwent dewaxing with xylene, and rehydration through various dilutions of ethanol and distilled water before being subjected to FJC staining, TUNEL staining, and immunofluorescence staining.

Fluoro-Jade C Staining

The Fluoro-Jade C (FJC) Ready-to-Dilute Staining Kit (TR-100-FJT, Biosensis, USA) was utilized to stain degenerated neurons in accordance with the manufacturer's instructions. [27]. Briefly, the sections were immersed in a 0.06% potassium permanganate solution for 10 min. After a 2-min rinse with distilled water, the sections were exposed to the FJC working solution and 4′,6-diamidino-2-phenylindole (DAPI) for 10 min. Subsequently, the sections were subjected to three 1-min washes with distilled water and subsequently dried on a slide warmer at 60 °C for a minimum of 5 min. Finally, the sections were placed in xylene for 5 min, coated with DPX (06522, Sigma-Aldrich, USA), and viewed using a fluorescence microscope (OLYMPUS, Japan). This process was conducted by two blinded observers with no knowledge of the experimental groups.

TUNEL Staining

Neuronal apoptosis was identified using the CF488 TUNEL Cell Apoptosis Detection Kit (G1504, Servicebio, Wuhan, China). The paraffin-embedded brain sections were treated with proteinase K solution (20 μg/mL) (ST532, Beyotime, China) at 37 °C for 20 min. After undergoing three rounds of PBS washing, with each wash lasting 10 min, the brain sections were subjected to incubation in a solution containing labeled nucleotides and TdT enzyme. This process was carried out in a dark environment at a temperature of 37 °C for a duration of 60 min. Afterward, the sections were subjected to incubation with a mouse anti-NeuN antibody (1:100, #94403, CST, USA) at 4 °C for 12 h. Following three washes with PBS, a secondary antibody conjugated with Alexa Fluor-594 (1:500, A23410, Abbkine, China) was administered at 37 °C for 60 min. DAPI staining (P0131, Beyotime, China) was employed for visualizing the nuclei. The results were presented as the proportion of neurons exhibiting TUNEL-positive staining.

Immunofluorescence Staining

Double immunofluorescence staining was conducted following the previously established protocol [26]. Antigen retrieval was accomplished through microwave heating for 28 min using a citrate antigen retrieval solution (P0083, Beyotime, China). Next, the sections were exposed to 0.1% Triton X-100 (GC204003, Servicebio, China) for 30 min and subsequently blocked with goat serum (AR0009, Boster, China) for 60 min. Following that, the sections were subjected to an overnight incubation at 4 °C with the primary antibodies listed below: mouse anti-NeuN (NeuN, #94403, 1:100, CST, USA), mouse anti-Iba-1 (Iba-1, 1:50, AiFang Biological, China), and mouse anti-GFAP (GFAP, #3670, 1:200, CST, USA), rabbit anti-GPR39 (#bs-5789R, 1:250, Bioss, China), rabbit TFAM (#22586–1-AP, 1:200, Proteintech, China), rabbit HO-1 (#380753, 1:100, ZEN BIO, China). After undergoing three rounds of PBS washing, the sections were subjected to the corresponding secondary antibodies (1:500, A23210/A23420, Abbkine, China) in a light-shielded environment at ambient temperature for one hour. The nuclei were subjected to DAPI staining (P0131, Beyotime Biotechnology, China) for a duration of 10 min. Finally, the sections were scrutinized, and images were captured using a fluorescence microscope (OLYMPUS, Japan) by an observer blinded to the conditions. The captured microphotographs were assessed with the assistance of ImageJ software.

Transmission Electron Microscopy

Transmission electron microscopy (TEM) was employed to investigate the structure and abundance of mitochondria. In brief, the mice were administered anesthesia and subsequently subjected to perfusion using a solution containing 4% paraformaldehyde and 2.5% glutaraldehyde. Then, brain

tissues of dimensions 1 × 1 × 1 mm were initially fixed in 2.5% glutaraldehyde and then underwent treatment with 1% osmic acid for further fixation. Next, the specimens underwent a series of ethanol concentration steps for dehydration. Following dehydration, the samples were infiltrated, embedded, and subsequently sliced into sections. Finally, the sections were subjected to a dual staining procedure involving 3% uranyl acetate and lead citrate before being examined under a transmission electron microscope (Hitachi, Japan).

Dihydroethidium (DHE) Staining

The Dihydroethidium (DHE) staining was conducted in order to assess the production of ROS within brain tissue. In brief, brain Sects. (10 μm) were rapidly frozen and then treated with the fluorescent dye dihydroethidium (DHE, D7008, Sigma-Aldrich, USA) at a concentration of 3 μmol/L. The incubation took place in a chamber with controlled humidity at 37 °C for 30 min while being shielded from light. Following two washes with PBS, the sections were exposed to DAPI (P0131, Beyotime Biotechnology, China) for a duration of 10 min and subsequently examined under a fluorescence microscope (OLYMPUS, Japan) by two researchers who were unaware of the experimental groups. The fluorescence intensity was quantified using ImageJ software.

Enzyme-linked Immunosorbent Assay

To measure crucial biomarkers linked to oxidative stress injury, we employed assay kits that were utilized following the guidelines provided by the manufacturer. MDA (#A007-1–1, NJJCBIO, Nanjing, China), SOD (#A001-3–2, NJJCBIO, Nanjing, China), CAT (#A007-1–1, NJJCBIO, Nanjing, China), and GSH-Px (#A005-1–2, NJJCBIO, Nanjing, China). In summary, peri-hematoma tissue samples were homogenized and combined with an extraction solution. The resulting mixture was then subjected to centrifugation at a temperature of 4 °C, and the resulting supernatants were evaluated for their respective absorbance using a microplate reader. Ultimately, the activity levels of the biomarkers were determined by employing appropriate formulas derived from the measured absorbance values.

Quantification of Mitochondrial DNA (mtDNA) Levels and ATP Content

The mtDNA copy number was evaluated via q-PCR, while the mtDNA content was determined by calculating the ratio of mtDNA to nuclear DNA (nDNA) [30]. The primer sequences utilized for amplifying both mtDNA and nDNA can be found in the Supporting File (Fig. S1). All the primes were synthesized by Sangon Biotech (Shanghai, China). In addition, the ATP levels were measured by employing the ATP Assay Kit (#A095-1–1, NJJCBIO, Nanjing, China), in accordance with the guidelines provided by the manufacturer.

Western Blot

We conducted Western blot analysis following the previously described protocol [31]. The samples were subjected to processing, and 20 μg of total protein from each sample underwent electrophoresis on an SDS gel. Subsequently, the proteins were transferred onto a PVDF membrane using electro-transfer techniques. The membrane was then blocked at a temperature of 37 °C for a duration of 1 h, followed by overnight incubation with primary antibodies at a temperature of 4 °C. The primary antibodies included rabbit anti-GPR39 (#bs-5789R, 1:2000, Bioss, China), rabbit anti-p-CREB (#ab32096, 1:5000, Abcam, USA), rabbit anti-CREB (#12208–1-AP, 1:500, Proteintech, China), rabbit anti-PGC-1α(#381615,1:500, ZEN BIO, China), rabbit anti-Nrf2(#12721S, 1:1000, CST, USA), mouse anti-NRF1(#12482–1-AP, 1:1000, Proteintech, China), rabbit anti-TFAM(#22586–1-AP, 1:2000, Proteintech, China), rabbit anti-HO-1(#380753, 1:500, ZEN BIO, China), rabbit anti-NQO1(#T56710, 1:1000, Abmart, China), rabbit anti-Bax(#CPA1091, 1:1000, Cohesion Biosciences, UK), rabbit anti-Bcl-2(#CPA1095, 1:1000, Cohesion Biosciences, UK), mouse anti-β-actin(#66009–1-ig, 1:20000, Proteintech, China). β-actin was utilized as an internal reference for normalizing the loading. After being washed three times with TBST, the bands were subsequently exposed to HRP-conjugated secondary antibodies (Goat Anti-Mouse/Rabbit IgG, #AS003/AS015, 1:5000, ABclone, China) for 60 min at room temperature. Subsequently, an ultra-high sensitivity ECL kit (GK10008, GLPBIO, USA) was utilized to visualize the immunoblots. Protein quantification was performed using ImageJ software.

Statistics Analysis

The mean ± standard deviation (mean ± SD) was used to present the data. No outlier test was conducted. GraphPad Prism 9 software (GraphPad, San Diego, CA) was employed for data analysis. The Shapiro–Wilk test was utilized as an initial step to assess the normality of the data. In the case of normal distribution, one-way analysis of variance (ANOVA) followed by Tukey's post hoc analysis was performed to detect intergroup statistical differences. If the data did not meet normality assumptions, Kruskal–Wallis one-way ANOVA on Ranks followed by Tukey's post hoc analysis was applied instead. Statistical significance was defined as a p-value below 0.05 ($p < 0.05$).

Results

Mortality and Exclusion

This study employed a total of 335 male C57/BL mice, with 56 in the sham group, 12 in the naive group, and 230 in the ICH group. Ten mice were excluded from this study due to the absence of hematoma. None of the mice in the sham group died during the study. The overall mortality among ICH mice in this study was 8.05% (27/335). There were no notable differences in the mortality rates observed among the groups under experimentation (Fig. S2).

Changes of Endogenous GPR39 Expression Following Experiment ICH in Mice

The endogenous GPR39 expression was assessed by Western blot, the data revealed a significant increase in the expression level of GPR39 in the peri-hematoma tissues at 24 h and 72 h in the ICH group when compared to the Sham group (Fig. 2A-B). To validate the subcellular localization of GPR39, a double immunofluorescence staining assay was conducted 24 h post-ICH. The results showed that GPR39 predominantly was expressed in neurons, microglia, and astrocytes (Fig. 2C).

Knockdown of Endogenous GPR39 Exacerbated Neurological Deficits at 72 h After ICH

To evaluate the impact of endogenous GPR39 on neurological behavior following ICH, GPR39 siRNA was administered into the lateral ventricles of mice 48 h prior to ICH induction, while mice from the same batch were injected with Scramble siRNA as a control. Western blot analysis revealed a significant reduction in GPR39 protein levels in naïve mice and ICH mice treated with GPR39 siRNA, confirming the efficacy of GPR39 knockdown by siRNA (Fig. 3A-B). The results of neurobehavioral function tests have shown that GPR39 knockdown aggravated the neurobehavioral deficits in mice with ICH (Fig. 3C-E).

TC-G 1008 iMproved Neurological Deficits, Decreased Brain Edema, and pRomoted Hematoma Absorption Following ICH in Mice

To assess the role of TC-G 1008 in brain injury and establish the optimal dosage and timing, three different doses were orally administered at 1 h, 25 h, and 49 h after ICH. Neurological behavior was evaluated at 24 h and 72 h after ICH using the modified Garcia test, corner turn test, and forelimb placement test. When compared to the Sham group, mice in the ICH + Vehicle group displayed notable neurological deficits at 24 h and 72 h. Treatment with TC-G 1008 (24 mg/kg) significantly improved neurological function, particularly at 72 h, compared to the TC-G 1008 (8 mg/kg) and TC-G 1008 (72 mg/kg) groups (Fig. 4A-C). Additionally, continuous administration of TC-G 1008 (24 mg/kg) at 1 h, 25 h, and 49 h post-ICH decreased brain edema and promoted hematoma absorption at 72 h after ICH (Fig. 4D-E). Based on these findings, we chose the optimal TC-G1008 dose (24 mg/kg) and the 72-h post-ICH time point for further exploration in subsequent experiments.

Treatment with TC-G 1008 Reduced the Neuronal Degeneration After ICH

The effect of TC-G 1008 on neuronal degeneration in the peri-hematoma tissues was investigated through FJC staining at 72 h after ICH. The number of FJC-positive neurons increased in the ICH + Vehicle group at 72 h after ICH compared with the Sham group. Treatment with TC-G 1008 reduced the number of FJC-positive neurons when compared with the ICH + Vehicle group. However, pretreatment with GPR39 siRNA significantly exacerbated neuronal degeneration when compared with ICH + TC-G 1008 + Scramble siRNA group (Fig. 5A-B).

Administration of TC-G 1008 Inhibited the Neuronal Apoptosis After ICH

To assess the potential effect of TC-G 1008 on neuronal apoptosis, Western blot, and TUNEL staining were employed at 72 h post-ICH. The Western blot results revealed that after ICH the expression of Bax was markedly elevated, while Bcl-2 expression was substantially reduced. Administration of TC-G 1008 increased Bcl-2 expression and decreased Bax expression compared with the ICH + Vehicle group. However, in contrast to the ICH + TC-G 1008 + Scramble siRNA group, pretreatment with GPR39 siRNA resulted in an upregulation of Bax expression and a downregulation of Bcl-2 expression (Fig. 6A-C). In line with western blot findings, TUNEL-positive neurons in the perihematomal area were markedly elevated in the ICH + Vehicle group compared to the Sham group at 72 h post-ICH. TC-G 1008 treatment reduced the number of TUNEL-positive neurons. In addition, pretreatment with GPR39 siRNA before ICH resulted in an increase in the number of TUNEL-positive neurons compared to the ICH + TC-G 1008 + Scramble siRNA group (Fig. 6D-E).

Treatment with TC-G 1008 Promoted Mitochondrial Biogenesis and Preserved Mitochondrial Structure After ICH

To determine the expression of molecules associated with mitochondrial biogenesis, Western blot analysis was

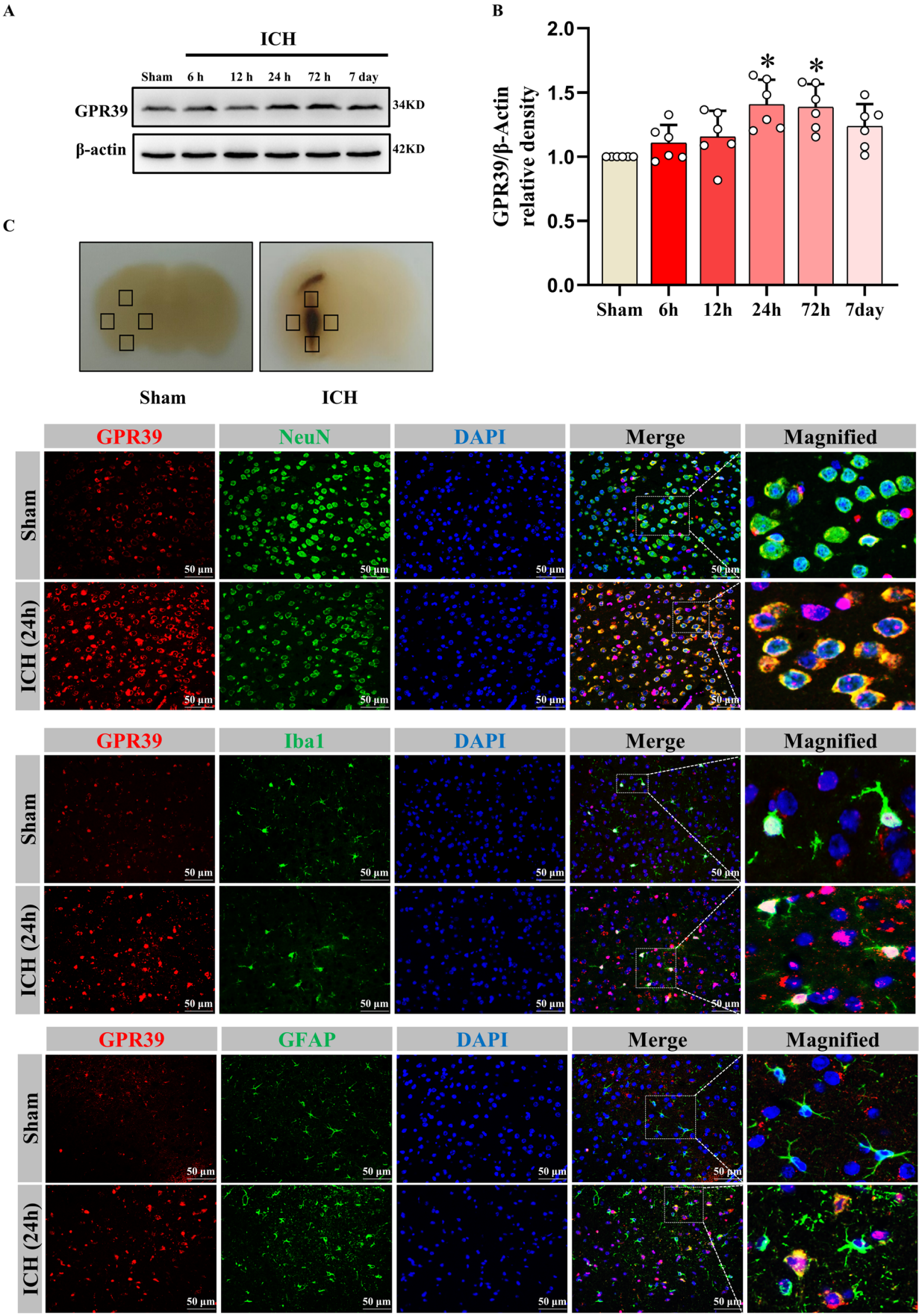
A
ICH
Sham
6 h
12 h
24 h
72 h
7 day
GPR39
34KD
β-actin
42KD
B
GPR39/β-Actin relative density
2.0
1.5
1.0
0.5
0.0
Sham
6h
12h
24h
72h
7day
C
Sham
ICH
GPR39
NeuN
DAPI
Merge
Magnified
Sham
ICH (24h)
50 μm
GPR39
Iba1
DAPI
Merge
Magnified
Sham
ICH (24h)
50 μm
GPR39
GFAP
DAPI
Merge
Magnified
Sham
ICH (24h)
50 μm

◂**Fig. 2** Time course and Cellular localization of endogenous GPR39 after ICH in mice. **A-B** Representative western blot band and quantitative analyses of GPR39 expression after ICH. Data was shown as Mean ± SD, $^{*}P < 0.05$ vs. Sham group. $n = 6$ per group. One-way ANOVA followed by Tukey's test. **C** Schematic diagram shows the peri-hematoma area for immunochemistry staining and western blot (black boxes) and representative images of double immunofluorescence staining demonstrated the co-localized of GPR39 (red) with neurons (NeuN, green), microglia (Iba1, green), astrocytes (GFAP, green) and DAPI (blue) separately at 24 h after ICH. Scale bar = 50 μm, $n = 3$ per group

performed. The expression of PGC-1α, NRF1, and TFAM was increased after ICH. Treatment with TC-G 1008 further upregulated expression of PGC-1α, NRF1, and TFAM compared to the ICH + Vehicle group. However, pretreatment of GPR39 siRNA significantly reversed the changes compared with the ICH + TC-G 1008 + Scramble siRNA group (Fig. 7A-D). In line with the Western blot results, the results of IF staining revealed that treatment with TC-G 1008 led to an increase in TFAM expression in neurons, while delivery of GPR39 siRNA reversed this change in TFAM expression compared to the ICH + TC-G 1008 + Scramble siRNA group (Fig. 7E-F).

In order to explore the effect of TC-G 1008 on the mitochondrial structure of neurons, TEM was performed. The results of TEM demonstrated that the mitochondria of neurons in the Sham group showed a long tubular appearance, with prominent cristae and intact membrane structure. ICH-induced neuronal mitochondrial swelling, dissolution, and a decrease in the number of structurally intact mitochondria. Treatment with TC-G 1008 partially reduced neuronal mitochondrial fragmentation and mitochondrial vacuolization, thereby

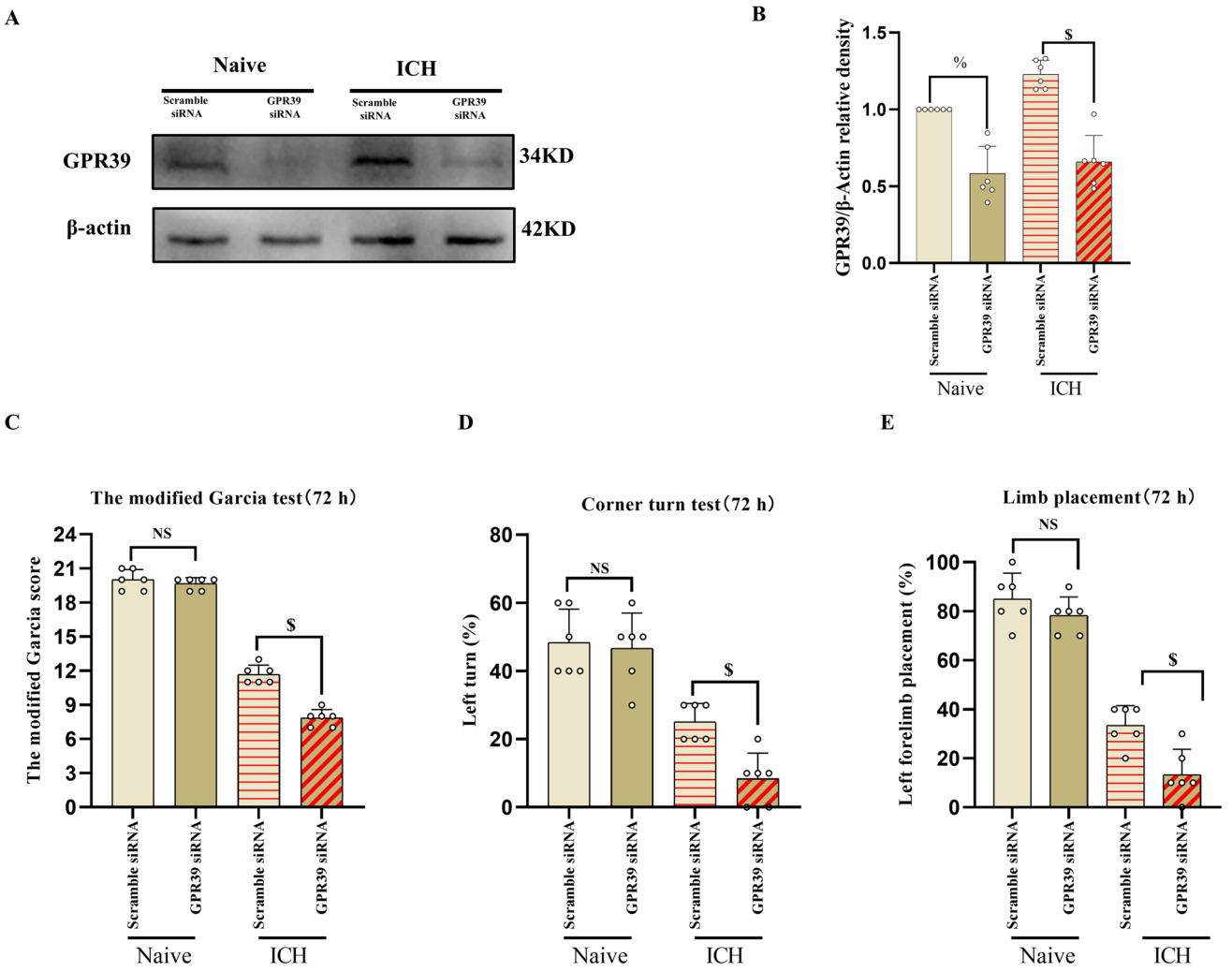

Fig. 3 Effects of GPR39 knockdown with siRNA on the level of GPR39 and neurological function at 72 h after ICH. **A-B** Representative Western blot bands of GPR39 after administration of GPR39 siRNA, and quantitative analyses of GPR39. **C–E** Modified Garcia test, forelimb placement test, and corner turn test at 72 h after surgery. Data was represented as mean ± SD. $^{\%}P < 0.05$ vs. Naïve + Scramble siRNA group. $^{\$}P < 0.05$ vs. ICH + Scramble siRNA group. $n = 6$ per group. One-way ANOVA followed by Tukey's test

preserving the integrity of mitochondrial morphology compared to the ICH + Vehicle group. However, in comparison to the ICH + TC-G 1008 + Scramble siRNA group, GPR39 siRNA abolished the beneficial effects of TC-G 1008 on the neuronal mitochondrial fragmentation and mitochondrial vacuolization following ICH (Fig. 7G-H).

In addition, the results of q-PCR and ELISA revealed a significant increase in the copy number of mtDNA replication and ATP content after TC-G 1008 treatment compared to the ICH + Vehicle group. However, these changes induced by TC-G 1008 were effectively reversed by GPR39 siRNA (Fig. 7I-J).

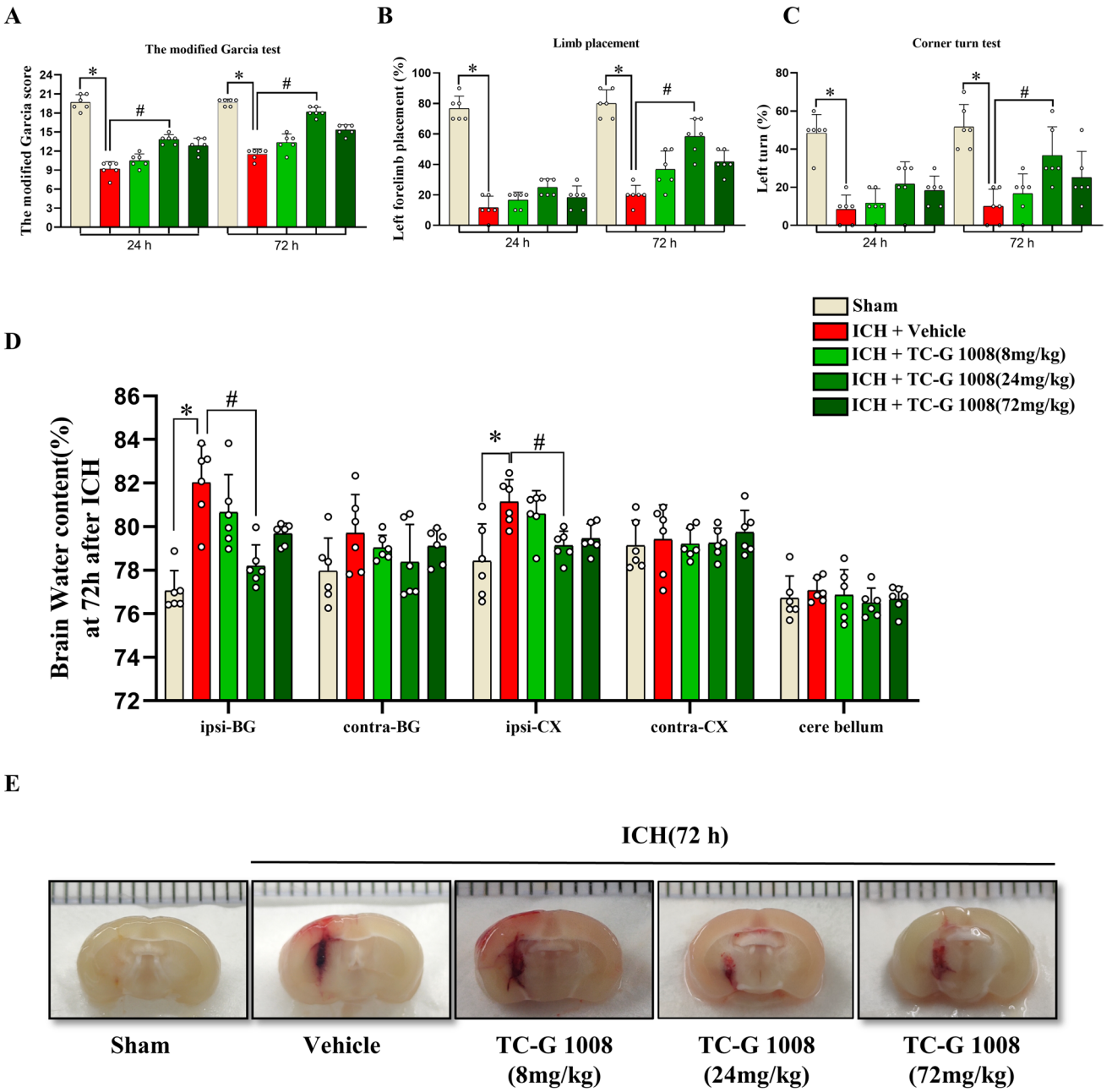

Fig. 4 The neuroprotective effect of TC-G 1008 on brain injury after ICH in mice. **A**-**C** TC-G 1008 (24 mg/kg) significantly improved neurobehavioral impairments. **D** TC-G 1008 (24 mg/kg) reduced brain water content at 72 h after ICH. **E** TC-G 1008 (24 mg/kg) promoted hematoma absorption at 72 h after ICH. Data was represented as mean ± SD. $^{*}P < 0.05$ vs. Sham group; $^{\#}P < 0.05$ vs. ICH + Vehicle group. $n = 6$ per group. One-way ANOVA followed by Tukey's test

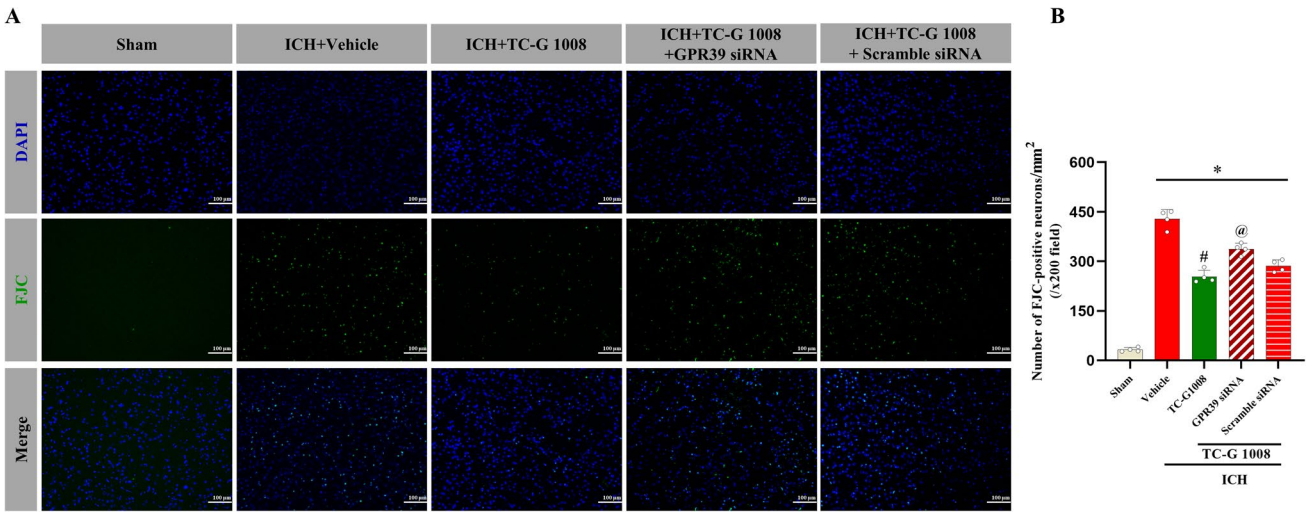

Fig. 5 Treatment with TC-G 1008 reduced the neuronal degeneration after ICH. **A-B** FJC staining and quantitative analyses. Data was represented as mean ± SD. $^{*}P < 0.05$ vs. Sham group; $^{\#}P < 0.05$ vs. ICH + Vehicle group; $^{@}P < 0.05$ vs. ICH + TC-G 1008 + Scramble siRNA group. $n = 4$ per group. One-way ANOVA followed by Tukey's test

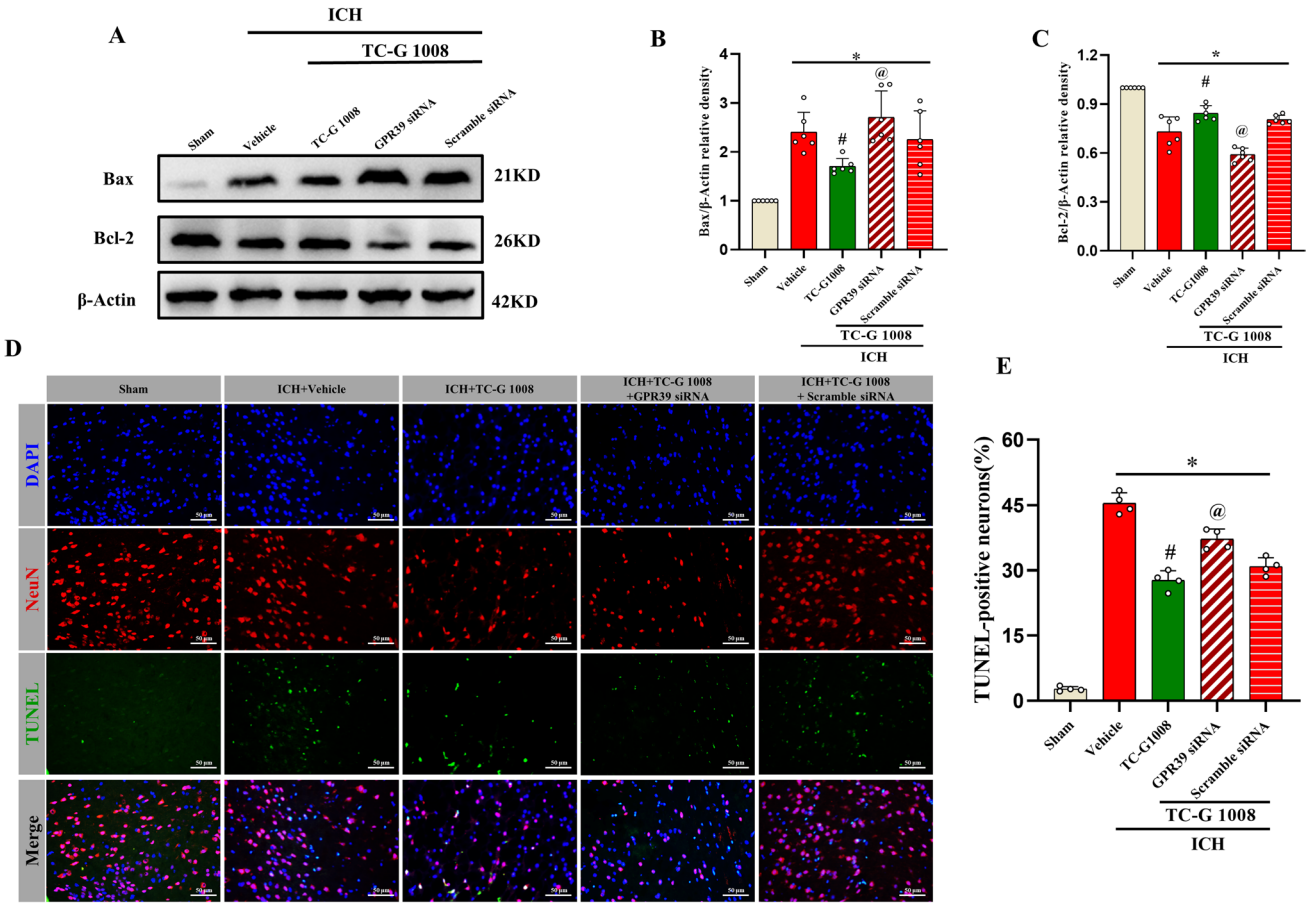

Fig. 6 Treatment with TC-G 1008 inhibited the neuronal apoptosis after ICH. **A**-**C** Representative Western blot and quantitative analyses of Bax and Bcl-2. $n = 6$ per group. D-E TUNEL staining and quantitative analyses. $n = 4$ per group. Data was represented as mean ± SD. $^{*}P < 0.05$ vs. Sham group; $^{\#}P < 0.05$ vs. ICH + Vehicle group; $^{@}P < 0.05$ vs. ICH + TC-G 1008 + Scramble siRNA group. One-way ANOVA followed by Tukey's test

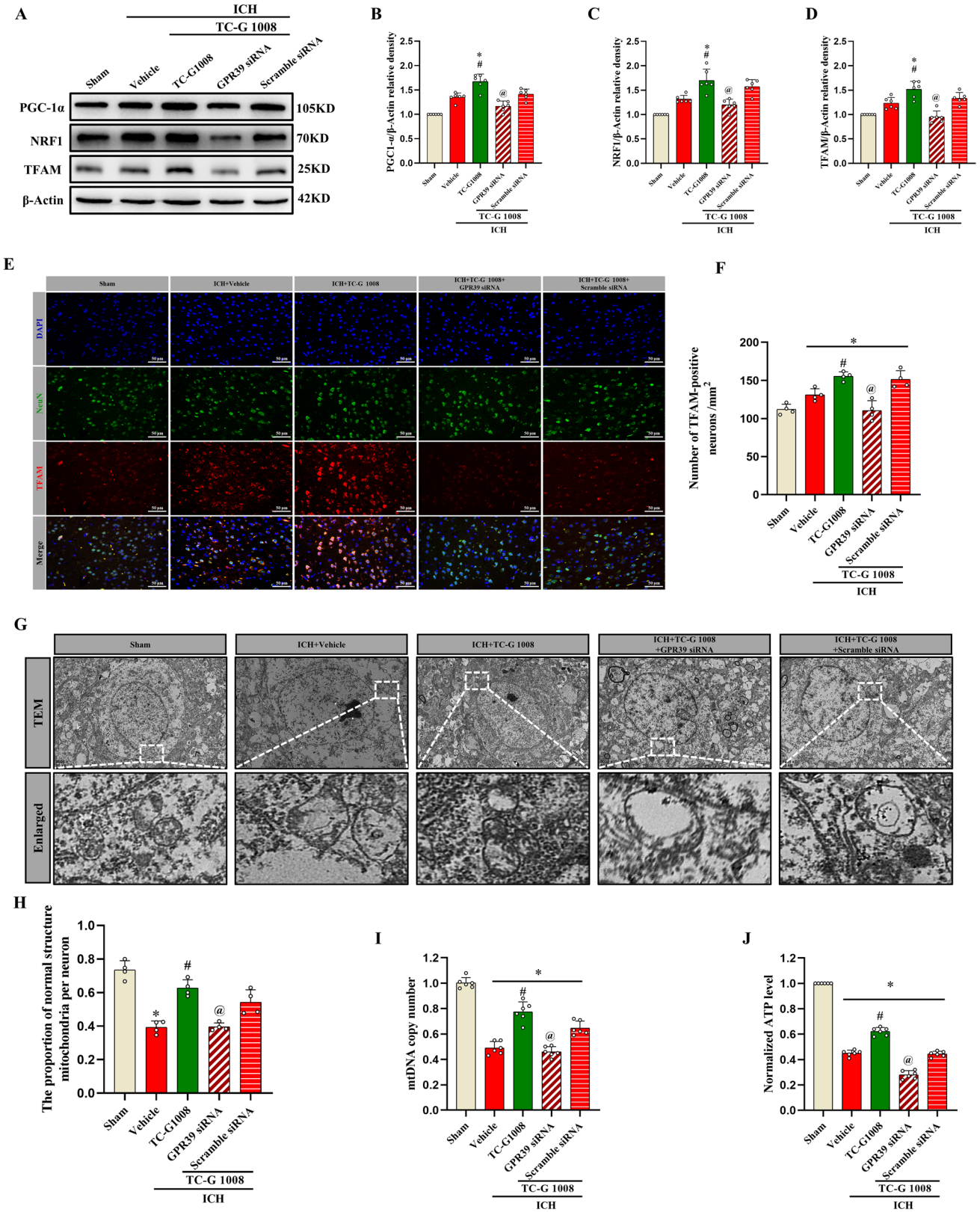
A
ICH
TC-G 1008
Sham
Vehicle
TC-G1008
GPR39 siRNA
Scramble siRNA
PGC-1α
NRF1
TFAM
β-Actin
105KD
70KD
25KD
42KD
B
PGC1-α/β-Actin relative density
C
NRF1/β-Actin relative density
D
TFAM/β-Actin relative density
E
Sham
ICH+Vehicle
ICH+TC-G 1008
ICH+TC-G 1008+ GPR39 siRNA
ICH+TC-G 1008+ Scramble siRNA
DAPI
NeuN
TFAM
Merge
F
Number of TFAM-positive neurons /mm2
G
TEM
Enlarged
ICH+TC-G 1008 +GPR39 siRNA
ICH+TC-G 1008 +Scramble siRNA
H
The proportion of normal structure mitochondria per neuron
I
mtDNA copy number
J
Normalized ATP level

◂**Fig. 7** Treatment with TC-G 1008 promoted mitochondrial biogenesis and preserved mitochondrial structure after ICH. **A-D** Representative Western blot and quantitative analyses of expression of PGC-1α, NRF1, and TFAM. $n=6$ per group. **E–F** Double immunofluorescence staining revealed the variations of TFAM (red) in the neuron (NeuN, green). $n=4$ per group. Scale bar = 50 μm. **G–H** Transmission electron microscope (TEM) of neuron and proportion of the number of normally structured mitochondria in a neuron. $n=4$ per group. Scale bar = 2 μm. **I-J** mtDNA copy number was detected by q-PCR and ATP content was detected by ELISA. $n=6$ per group. Data was represented as mean ± SD. $^{*}P<0.05$ vs. Sham group; $^{\#}P<0.05$ vs. ICH + Vehicle group; $^{@}P<0.05$ vs. ICH + TC-G 1008 + Scramble siRNA group. One-way ANOVA followed by Tukey's test

TC-G 1008 Treatment Improved the Antioxidative Capability after ICH

To investigate whether TC-G1008 could regulate the antioxidative capability after ICH, Western blot, DHE staining, and ELISA were performed at 72 h after ICH. Western blot results showed that the expression of endogenous antioxidative stress-related molecules including Nrf2 and HO-1 was upregulated, compared with the Sham group. Continuous administration of TC-G 1008 not only further increased the expression of Nrf2 and HO-1, but also enhanced the expression of NQO1 compared to the ICH + Vehicle group at 72 h post-ICH. However, pretreatment with GPR39 siRNA resulted in a reduction in the expression of Nrf2, HO-1, and NQO1 compared to the ICH + TC-G 1008 + Scramble siRNA group (Fig. 8A-D). In addition, DHE staining results showed that the ROS levels around the peri-hematoma were significantly increased after ICH, but administration of TC-G 1008 effectively attenuated the ROS levels. Moreover, the levels of ROS were higher in the ICH + TC-G 1008 + GPR39 siRNA group compared to the ICH + TC-G 1008 + Scramble siRNA group (Fig. 8E-F).

ELISA results showed that the MDA level was increased, and the levels of SOD, CAT, and GSH-Px were decreased in the peri-hematoma tissues after ICH. Treatment with TC-G 1008 dramatically increased the activities of SOD, CAT, and GSH-Px and markedly decreased the MDA level compared with the ICH + Vehicle group. Nevertheless, pretreatment with GPR39 siRNA resulted in a higher level of MDA, as well as diminished activities of SOD, CAT, and GSH-Px compared to the ICH + TC-G 1008 + Scramble siRNA group (Fig. 8G-J).

Inhibition of CREB Reversed Protective Effects of TC-G 1008 After ICH

To explore whether the protective effects of TC-G 1008 are related to the CREB/PGC-1α pathway, a specific inhibitor of CREB, 666–15, was administered 24 h prior to ICH induction. The results of neurobehavioral function tests indicated that CREB inhibitor exacerbated neurobehavioral deficits at 72 h post-ICH compared to the ICH + TC-G 1008 + Vehicle 2 group (Fig. 9A-C). Western blot analysis showed that 666–15 markedly decreased the expression of p-CREB, PGC-1α, NRF1, TFAM, Nrf2, HO-1, and NQO1 in the peri-hematoma tissues (Fig. 9D-K). In addition, IF staining also confirmed that the CREB inhibitor indeed reduced the expression of HO-1 in neurons compared to the ICH + TC-G 1008 + Vehicle 2 group. (Fig. 9L-M). We conducted ELISA to investigate the effect of 666–15 on antioxidant capacity induced by TC-G1008 after ICH. The results showed that compared with the ICH + TC-G 1008 + Vehicle 2 group, the level of MDA was significantly increased, and the activities of SOD, CAT, and GSH-Px were decreased (Fig. 9N-Q). Moreover, the q-PCR and ELISA results also indicated a decrease in mtDNA copy number and ATP content compared to the ICH + TC-G 1008 + Vehicle 2 group (Fig. 9R-S).

Discussion

After ICH, the red blood cell lysate products, iron overload, and other injurious factors lead to a series of complex pathological processes, which have not been fully elucidated [32, 33]. Neuronal mitochondrial dysfunction and oxidative stress injury are considered important causes of brain injury post-ICH [34]. In the present study, we demonstrated that treatment with TC-G1008 (a specific GPR39 agonist) could regulate neuronal mitochondrial biogenesis and antioxidative capability against ICH-induced SBI (Fig. 10).

We found that the endogenous GPR39 expression level remarkably increased at an early stage following experimental ICH in mice, predominantly colocalized in neurons and microglia in the peri-hematoma tissues. Activation of GPR39 with TC-G1008 significantly improved neurological deficits, diminished brain edema, promoted hematoma absorption, and alleviated neuronal degeneration and apoptosis after ICH. In addition, TC-G 1008 treatment promoted neuronal mitochondrial biogenesis and enhanced antioxidative capability. Furthermore, the CREB inhibitor partially reversed the neuroprotective effects of TC-G 1008 after ICH. Taken together, our findings indicated that GPR39 agonist TC-G 1008 has the potential to promote mitochondrial biogenesis and improve antioxidative capability after ICH, which is at least in part mediated by CREB/PGC-1α pathway.

Mitochondria, which are responsible for energy generation, oxygen-free radical production, and cell apoptosis, contribute significantly to neuronal function and survival [35]. Importantly, energy production in neuronal cells relies entirely on mitochondrial oxidative phosphorylation, making them highly susceptible to disruptions caused by mitochondrial dysfunction [36]. There is an increasing amount

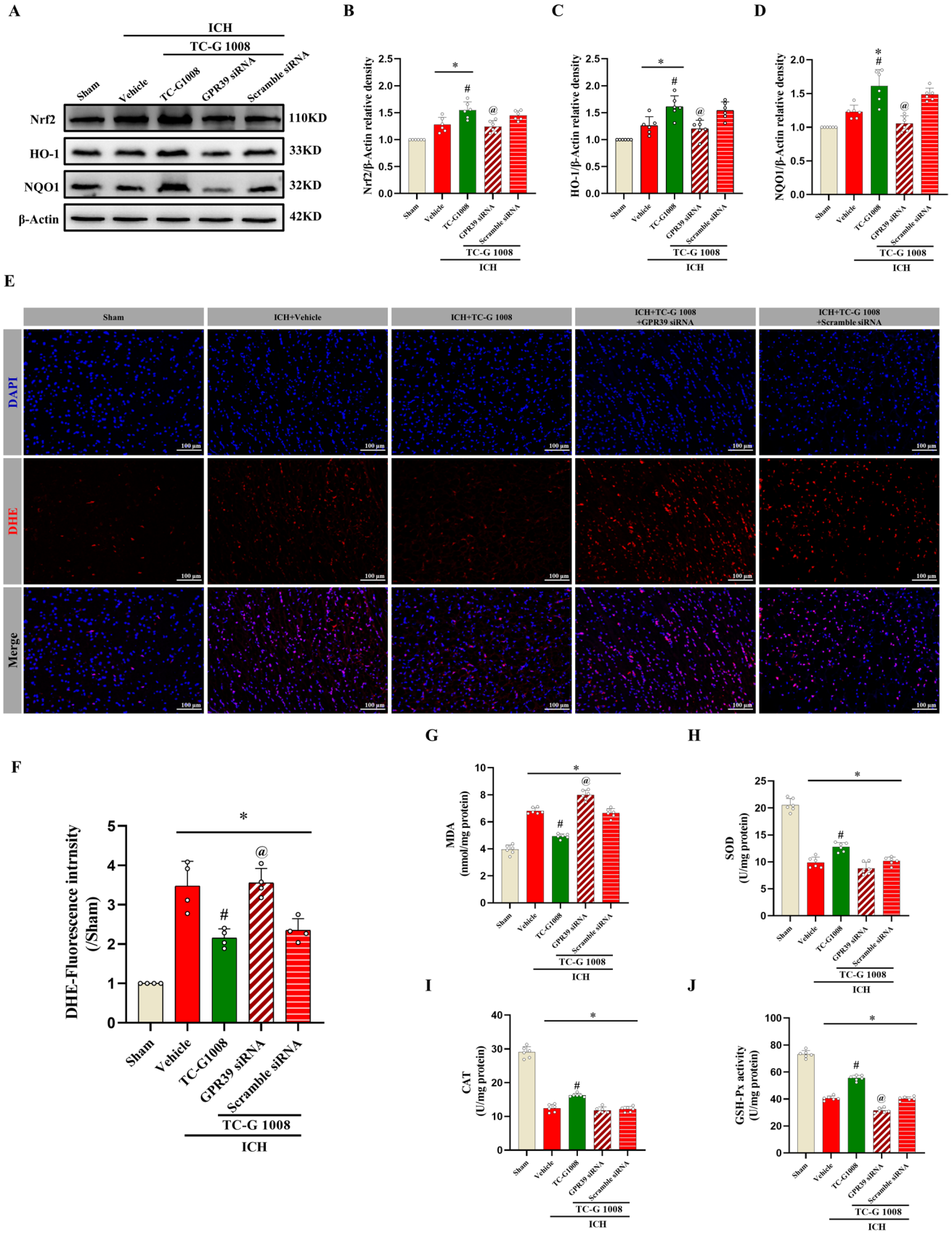
A
ICH
TC-G 1008
Sham
Vehicle
TC-G1008
GPR39 siRNA
Scramble siRNA
Nrf2
HO-1
NQO1
β-Actin
110KD
33KD
32KD
42KD
B
Nrf2/β-Actin relative density
C
HO-1/β-Actin relative density
D
NQO1/β-Actin relative density
E
Sham
ICH+Vehicle
ICH+TC-G 1008
ICH+TC-G 1008 +GPR39 siRNA
ICH+TC-G 1008 +Scramble siRNA
DAPI
DHE
Merge
100 μm
F
DHE-Fluorescence intrnsity (/Sham)
G
MDA (nmol/mg protein)
H
SOD (U/mg protein)
I
CAT (U/mg protein)
J
GSH-Px activity (U/mg protein)

◂**Fig. 8** Treatment with TC-G 1008 improved antioxidative capability after ICH. **A**-**D** Representative Western blot and quantitative analyses of expression of Nrf2, HO-1, and NOQ1. $n = 6$ per group. **E**–**F** DHE staining was used to detect the ROS levels in each group after ICH. $n = 4$ per group. Scale bar = 100 μm. **G**-**J** MDA, SOD, CAT levels and GSH-Px activity in the peri-hematoma tissues were detected by ELISA after ICH. $n = 6$ per group. Data was represented as mean ± SD. $^{*}P < 0.05$ vs. Sham group; $^{\#}P < 0.05$ vs. ICH + Vehicle group; $^{@}P < 0.05$ vs. ICH + TC-G 1008 + Scramble siRNA group. One-way ANOVA followed by Tukey's test

of evidence suggesting that mitochondrial dysfunction plays a significant role in the development of SBI after ICH [37]. Specifically, mitochondrial dysfunction can give rise to neuronal apoptosis and necrosis through various mechanisms. Following ICH, the release of free radicals from damaged mitochondria leads to an excessive production of ROS and oxidative damage to brain [38]. Moreover, mitochondria with abnormal structure and morphology can cause inadequate ATP production, cytotoxic edema, and cell death after ICH [39]. In the current study, we observed an increase in ROS production, and Bax expression, with a decrease in Bcl-2 expression after ICH. Consistent with previous research, we also found that ICH leads to a large number of neuronal apoptosis. Moreover, neuronal mitochondria displayed swelling and dissolution, along with a reduced number of intact mitochondria. Additionally, both ATP content and mtDNA replication copy number decreased. These findings also indicated that ICH-induced mitochondrial dysfunction is probably accompanied with neuronal apoptosis.

TC-G 1008, a potent GPR39 agonist, participates in various biological activities including anti-apoptosis, anti-inflammation, hepatoprotection, and neuroprotection [22, 40–42]. In the central nervous system, TC-G 1008 was reported to attenuate neuroinflammation after neonatal hypoxic–ischemic injury in rats [23]. Moreover, Doboszewska U et al. discovered that TC-G 1008 facilitates epileptogenesis by acting selectively at the GPR39 receptor in the hippocampus of pentylenetetrazole-kindled mice. Herein, our results showed that treatment with TC-G 1008 significantly improved short-term neurological deficits, decreased brain edema, and promoted hematoma absorption after ICH. The neuronal apoptosis in perihematomal tissue was significantly reduced by the use of TC-G 1008. Thus, these findings preliminary confirmed the neuroprotective effects of TC-G 1008 against neuronal injury.

Recent studies indicate that impaired mitochondrial biogenesis contributes to both mitochondrial dysfunction and excessive ROS production [10]. Li et al. demonstrated that activation of Aldehyde dehydrogenase 2 (ALDH2) enhanced PGC-1α-mediated mitochondrial biogenesis and alleviated mitochondrial dysfunction in acute kidney injury [43]. In addition, pre-treating rat brain cells with quercetin reduced ROS production by promoting mitochondrial biogenesis [44]. Moreover, previous studies demonstrated that enhancing mitochondrial biogenesis could restore mitochondrial function and mitigate brain injury after traumatic brain injury (TBI) and subarachnoid hemorrhage (SAH) [14, 45]. Intriguingly, a recent study has shown that TC-G 1008 has the ability to protect mitochondrial function and mitigate oxidative stress in the context of rheumatoid arthritis, and Zhang et al. found that TC-G 1008 can effectively promote neuronal mitochondrial biogenesis in neuropathic pain rat model [46, 47]. In our study, the results also showed that TC-G 1008 treatment significantly increased nascent neuronal mitochondria, with reduced fragmentation and vacuolization after ICH. Moreover, treatment with TC-G 1008 resulted in a significant increase in mtDNA copy number and ATP production with reduced ROS generation. Additionally, TC-G 1008 upregulated the expression of molecules associated with mitochondrial biogenesis, including PGC-1α, NRF1, and TFAM after ICH. Therefore, our findings suggested that the neuroprotective effects of TC-G 1008 in ICH mice are probably mediated by promoting mitochondrial biogenesis, mitigating mitochondrial dysfunction, and reducing ROS overproduction.

Excessive production of ROS has been recognized as the primary factor contributing to the oxidative stress response following acute brain injury [29]. In cases where the endogenous antioxidant system fails to efficiently eliminate ROS, it further exacerbates oxidative stress. Significantly, an overabundance of oxidative stress has the potential to trigger neuronal apoptosis, a prominent characteristic of SBI [48]. Growing evidence suggested that strategies to boost antioxidative capacity could improve outcomes after ICH [49]. Previous research displayed that TC-G 1008 can play an antioxidative role in multiple disease models [47, 50]. In line with prior research, treatment with TC-G 1008 significantly improved antioxidative capacity after ICH, as evidenced by increased levels of anti-ROS markers, such as SOD, CAT, and GSH-Px. Furthermore, treatment with TC-G 1008 increased the expression of antioxidative stress-related molecules, such as Nrf2, HO-1, and NQO1. Consequently, these findings further implied that TC-G 1008 treatment also improved antioxidative capacity after ICH.

Subsequently, we explored the underlying mechanism and signaling pathway responsible for TC-G 1008-induced mitochondrial biogenesis and enhanced antioxidative capacity. A previous study showed that TC-G 1008 protected against corticosterone-induced neuronal injury by activating the CREB signaling pathway [22]. CREB, a transcriptional co-factor with binding sequences on multiple promoters, initiated transcriptional cascades that were involved in various processes, including mitochondrial biogenesis [10, 51]. PGC-1α promoter and specific mitochondrial genes, including ND2, ND4, and ND5, harbor a CREB binding sequence [52]. Furthermore, Zhao

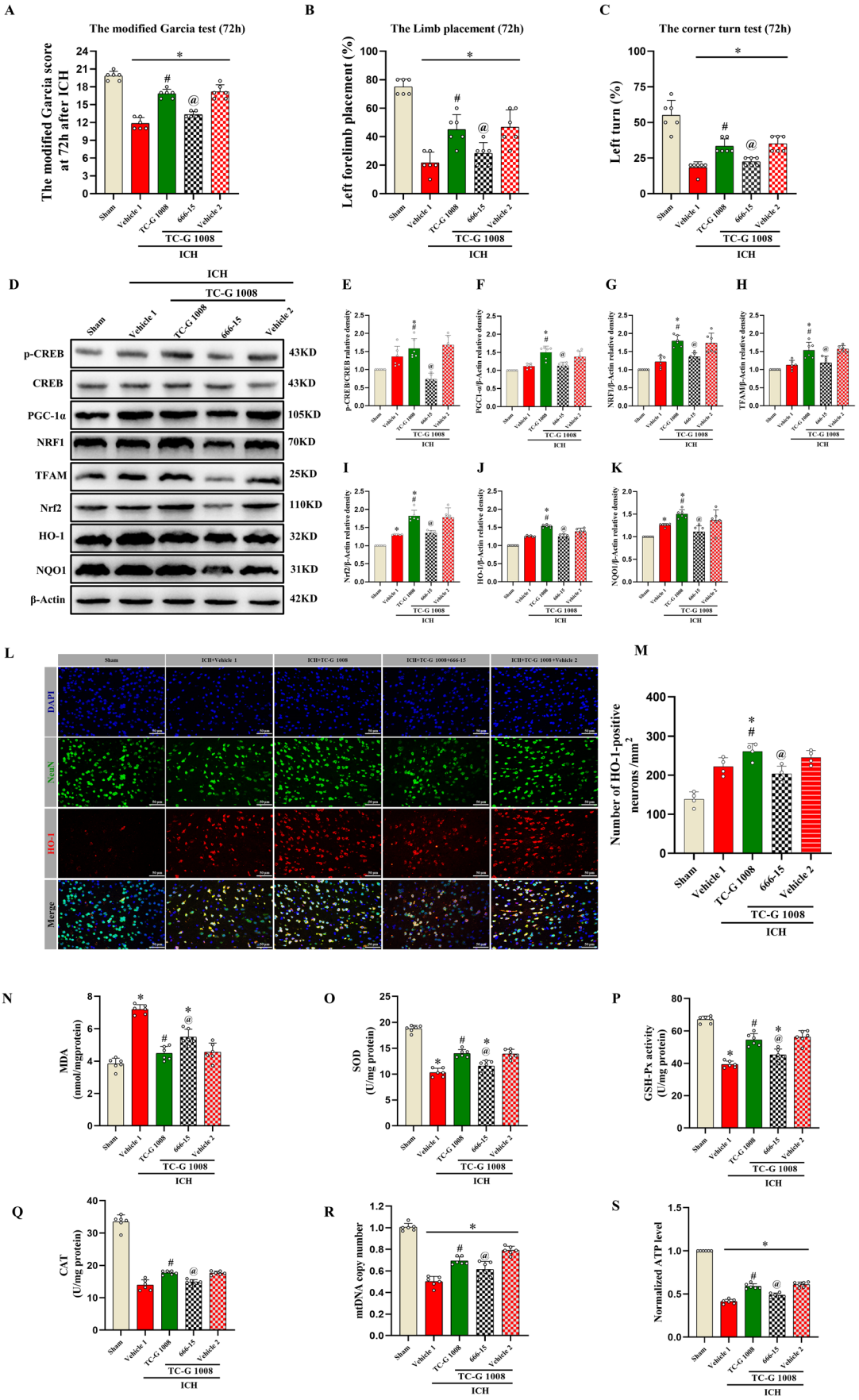
A
The modified Garcia test (72h)
The modified Garcia score at 72h after ICH
B
The Limb placement (72h)
Left forelimb placement (%)
C
The corner turn test (72h)
Left turn (%)
Sham
Vehicle 1
TC-G 1008
666-15
Vehicle 2
TC-G 1008
ICH
D
p-CREB 43KD
CREB 43KD
PGC-1α 105KD
NRF1 70KD
TFAM 25KD
Nrf2 110KD
HO-1 32KD
NQO1 31KD
β-Actin 42KD
E
p-CREB/CREB relative density
F
PGC1-α/β-Actin relative density
G
NRF1/β-Actin relative density
H
TFAM/β-Actin relative density
I
Nrf2/β-Actin relative density
J
HO-1/β-Actin relative density
K
NQO1/β-Actin relative density
L
Sham
ICH+Vehicle 1
ICH+TC-G 1008
ICH+TC-G 1008+666-15
ICH+TC-G 1008 +Vehicle 2
DAPI
NeuN
HO-1
Merge
M
Number of HO-1-positive neurons /mm2
N
MDA (nmol/mgprotein)
O
SOD (U/mg protein)
P
GSH-Px activity (U/mg protein)
Q
CAT (U/mg protein)
R
mtDNA copy number
S
Normalized ATP level

◂**Fig. 9** Inhibition of CREB with 666–15 reversed protective effects of TC-G 1008 on neuronal mitochondrial biogenesis and antioxidative capability after ICH. **A-C** Modified Garcia test, forelimb placement test, and corner turn test at 72 h. $n=6$ per group. **D-K** Representative Western blot and quantitative analyses of expression of p-CREB, CREB, PGC-1α, NRF1, TFAM, Nrf2, HO-1, and NQO1. $n=6$ per group. **L-M** Double immunofluorescence staining revealed the variations of HO-1 (red) in the neuron (NeuN, green). $n=4$ per group. Scale bar = 50 μm. **N-Q** MDA, SOD, CAT levels and GSH-Px activity in the peri-hematoma tissues were detected by ELISA after ICH. $n=6$ per group. **R-S** mtDNA copy number was detected by q-PCR and ATP content was detected by ELISA. $n=6$ per group. Data was represented as mean ± SD. $^{*}P<0.05$ vs Sham group; $^{\#}P<0.05$ vs ICH + Vehicle 1 group; $^{@}P<0.05$ vs ICH + TC-G 1008 + Vehicle 2 group. One-way ANOVA followed by Tukey's test

et al. have demonstrated that the CREB/PGC-1α signaling pathway in endothelial cells promoted mitochondrial biogenesis through the activation of G protein-coupled receptor (TGR5) [53]. Importantly, previous studies have also suggested that activating CREB provides neuroprotection by suppressing oxidative stress and ameliorating neuroinflammation in the ICH mouse model [28, 54]. Consistent with previous studies, our results showed that the neuroprotective effects of TC-G 1008 were effectively reversed by the administration of 666–15, associated with the alterations in PGC-1α, NRF1, Nrf2, TFAM, HO-1, and NQO1. Therefore, these findings further confirmed our hypothesis that activation of GPR39 with TC-G 1008 could promote

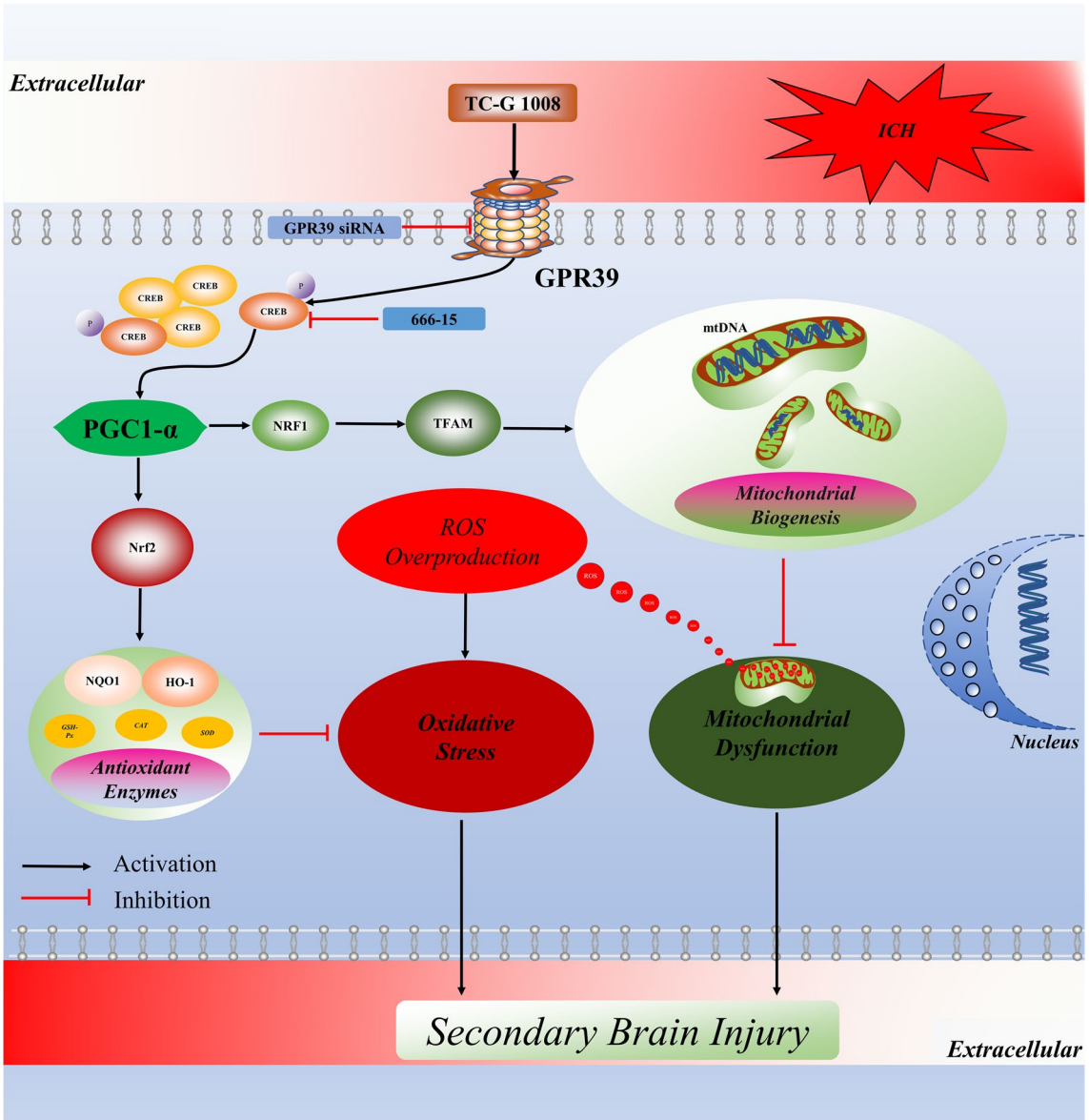

Fig. 10 Schematic diagram of potential molecular mechanisms of the neuroprotective effect of GPR39 agonist TC-G 1008 through the CREB/PGC-1α pathway after ICH

mitochondrial biogenesis and improve antioxidative capability, partially through the CREB/PGC-1α signaling pathway.

Despite these positive results, the current study has several limitations. Firstly, there have been reports that TC-G 1008 exhibits numerous biological characteristics, we only focused on mitochondrial biogenesis and antioxidative stress in neurons after ICH, the effect of TC-G 1008 on neuroinflammation after ICH should also be explored. Secondly, it is imperative to consider the potential involvement of alternative molecular signaling pathways that may contribute to the advantageous effects of TC-G 1008. Lastly, a comprehensive analysis of the long-term effects and fundamental mechanisms of TC-G 1008 should be conducted in the future.

Conclusion

The current study suggested that TC-G 1008 promoted mitochondrial biogenesis and improved antioxidative capability after experimental ICH in mice, potentially mediated by activating GPR39 and its downstream CREB/ PGC-1α signaling pathway. Therefore, GPR39 agonist TC-G 1008 may exert a promising therapeutic agent for mitigating brain injury in patients with ICH.

Supplementary Information The online version contains supplementary material available at https://doi.org/10.1007/s12975-024-01240-1.

Author Contributions The research was conceived and designed by Zhongyi Zhang and Lingui Gu. Zhongyi Zhang, Xingyu Zhang, and Jinyu Dai conducted the research. Ye Yuan and Yuguang Tang analyzed the data. Zhongyi Zhang, Yutong Zhao, Yihao Tao, and Zongyi Xie drafted and revised the manuscript. All authors have reviewed and approved the final version of the manuscript.

Funding This work was supported by the National Natural Science Foundation of China (No. 82201470), Chongqing Natural Science Foundation Project (No. CSTB2023NSCQ-MSX0107 and No. cstc2020jcyj-msxmX0225), and Chongqing Postdoctoral Science Foundation (No.2022CQBSHTB3097).

Data Availability The data used in the present study are available from the corresponding author upon reasonable request.

Declarations

Ethics Approval and Consent to Participate This research study strictly followed the guidelines established by the United States National Institutes of Health for the care and utilization of laboratory animals. Prior to commencing any testing or experimental procedures, comprehensive evaluations were conducted on the study protocols and obtained approval from Chongqing Medical University's Animal Ethics Committee (Permit number: IACUG-CQMU-2022–0015).

Competing Interests The authors declare no competing interests.

References

1. Cordonnier C, Demchuk A, Ziai W, Anderson CS. Intracerebral haemorrhage: current approaches to acute management. Lancet. 2018;392(10154):1257–68. https://doi.org/10.1096/fj.11-184531.
2. Chen Y, Chen S, Chang J, Wei J, Feng M, Wang R. Perihematomal edema after intracerebral hemorrhage: an update on pathogenesis, risk factors, and therapeutic advances. Front Immunol. 2021;12:740632. https://doi.org/10.3389/fimmu.2021.740632.
3. Li Y, Liu H, Tian C, An N, Song K, Wei Y, Sun Y, Xing Y, Gao Y. Targeting the multifaceted roles of mitochondria in intracerebral hemorrhage and therapeutic prospects. Biomed Pharmacother. 2022;148:112749. https://doi.org/10.1016/j.biopha.2022.112749.
4. Zheng Y, Li R, Fan X. Targeting oxidative stress in intracerebral hemorrhage: prospects of the natural products approach. Antioxidants (Basel). 2022;11(9). https://doi.org/10.3390/antiox11091811
5. Simmons EC, Scholpa NE, Schnellmann RG. Mitochondrial biogenesis as a therapeutic target for traumatic and neurodegenerative CNS diseases. Exp Neurol. 2020;329:113309. https://doi.org/10.1016/j.expneurol.2020.113309.
6. Zhang Y, Khan S, Liu Y, Wu G, Yong VW, Xue M. Oxidative stress following intracerebral hemorrhage: from molecular mechanisms to therapeutic targets. Front Immunol. 2022;13:847246. https://doi.org/10.3389/fimmu.2022.847246.
7. Popov L-D. Mitochondrial biogenesis: an update. J Cell Mol Med. 2020;24(9):4892–9. https://doi.org/10.1111/jcmm.15194.
8. Scarpulla RC. Transcriptional paradigms in mammalian mitochondrial biogenesis and function. Physiol Rev. 2008;88(2):611–38. https://doi.org/10.1152/physrev.00025.2007.
9. Kummer E, Ban N. Mechanisms and regulation of protein synthesis in mitochondria. Nat Rev Mol Cell Biol. 2021;22(5):307–25. https://doi.org/10.1038/s41580-021-00332-2.
10. Bouchez C, Devin A. Mitochondrial biogenesis and mitochondrial reactive oxygen species (ROS): a complex relationship regulated by the cAMP/PKA signaling pathway. Cells. 2019;8(4). https://doi.org/10.3390/cells8040287
11. Bi J, Zhang J, Ren Y, Du Z, Li Q, Wang Y, Wei S, Yang L, Zhang J, Liu C, et al. Irisin alleviates liver ischemia-reperfusion injury by inhibiting excessive mitochondrial fission, promoting mitochondrial biogenesis and decreasing oxidative stress. Redox Biol. 2019;20:296–306. https://doi.org/10.1016/j.redox.2018.10.019.
12. Yu H, Zhang F, Yan P, Zhang S, Lou Y, Geng Z, Li Z, Zhang Y, Xu Y, Lu Y, et al. LARP7 protects against heart failure by enhancing mitochondrial biogenesis. Circulation. 2021;143(20):2007–22. https://doi.org/10.1161/CIRCULATIONAHA.120.050812.
13. Chen Y, Yang Y, Liu Z, He L. Adiponectin promotes repair of renal tubular epithelial cells by regulating mitochondrial biogenesis and function. Metabolism. 2022;128:154959. https://doi.org/10.1016/j.metabol.2021.154959.
14. Fan H, Ding R, Liu W, Zhang X, Li R, Wei B, Su S, Jin F, Wei C, He X, et al. Heat shock protein 22 modulates NRF1/TFAM-dependent mitochondrial biogenesis and DRP1-sparked mitochondrial apoptosis through AMPK-PGC1α signaling pathway to alleviate the early brain injury of subarachnoid hemorrhage in rats. Redox Biol. 2021;40:101856. https://doi.org/10.1016/j.redox.2021.101856.
15. Egerod KL, Holst B, Petersen PS, Hansen JB, Mulder J, Hökfelt T, Schwartz TW. GPR39 splice variants versus antisense gene LYPD1: expression and regulation in gastrointestinal tract, endocrine pancreas, liver, and white adipose tissue. Mol Endocrinol. 2007;21(7):1685–98. https://doi.org/10.1096/fj.11-184531.
16. Petersen PS, Jin C, Madsen AN, Rasmussen M, Kuhre R, Egerod KL, Nielsen LB, Schwartz TW, Holst B. Deficiency of the GPR39 receptor is associated with obesity and altered adipocyte

metabolism. FASEB J. 2011;25(11):3803–14. https://doi.org/10.1096/fj.11-184531.
17. Ishitobi Y, Akiyoshi J, Honda S, Ninomiya T, Kanehisa M, Tanaka Y, Tsuru J, Isogawa K, Kitamura H, Fujikura Y. Administration of antisense DNA for GPR39-1b causes anxiolytic-like responses and appetite loss in rats. Neurosci Res. 2012;72(3):257–62. https://doi.org/10.1016/j.neures.2011.12.002.
18. Sunuwar L, Medini M, Cohen L, Sekler I, Hershfinkel M. Correction to 'The zinc sensing receptor, ZnR/GPR39, triggers metabotropic calcium signalling in colonocytes and regulates occludin recovery in experimental colitis'. Philos Trans R Soc Lond B Biol Sci. 2016;371(1703). https://doi.org/10.1098/rstb.2016.0331.
19. Jiang Y, Li T, Wu Y, Xu H, Xie C, Dong Y, Zhong L, Wang Z, Zhao H, Zhou Y, et al. GPR39 overexpression in OSCC Promotes YAP-sustained malignant progression. J Dent Res. 2020;99(8):949–58. https://doi.org/10.1177/0022034520915877.
20. Satianrapapong W, Pongkorpsakol P, Muanprasat C. A G-protein coupled receptor 39 agonist stimulates proliferation of keratinocytes via an ERK-dependent pathway. Biomed Pharmacother. 2020;127:110160. https://doi.org/10.1016/j.biopha.2020.110160.
21. Farbood Y, Sarkaki A, Mahdavinia M, Ghadiri A, Teimoori A, Seif F, Dehghani MA, Navabi SP. Protective effects of co-administration of zinc and selenium against streptozotocin-induced alzheimer's disease: behavioral, mitochondrial oxidative stress, and GPR39 expression alterations in rats. Neurotox Res. 2020;38(2):398–407. https://doi.org/10.1007/s12640-020-00226-9.
22. Mo F, Tang Y, Du P, Shen Z, Yang J, Cai M, Zhang Y, Li H, Shen H. GPR39 protects against corticosterone-induced neuronal injury in hippocampal cells through the CREB-BDNF signaling pathway. J Affect Disord. 2020;272:474–84. https://doi.org/10.1016/j.jad.2020.03.137.
23. Xie S, Jiang X, Doycheva DM, Shi H, Jin P, Gao L, Liu R, Xiao J, Hu X, Tang J, et al. Activation of GPR39 with TC-G 1008 attenuates neuroinflammation via SIRT1/PGC-1α/Nrf2 pathway post-neonatal hypoxic-ischemic injury in rats. J Neuroinflammation. 2021;18(1):226. https://doi.org/10.1186/s12974-021-02289-7.
24. Xu Y, Zhang WH, Allen EM, Fedorov LM, Barnes AP, Qian ZY, Bah TM, Li Y, Wang RK, Shangraw RE, et al. GPR39 knockout worsens microcirculatory response to experimental stroke in a sex-dependent manner. Transl Stroke Res. 2023;14(5):766–75. https://doi.org/10.1007/s12975-022-01093-6.
25. Imai T, Matsubara H, Hara H. Potential therapeutic effects of Nrf2 activators on intracranial hemorrhage. J Cereb Blood Flow Metab. 2021;41(7):1483–500. https://doi.org/10.1177/0271678X20984565.
26. Gu L, Sun M, Li R, Tao Y, Luo X, Xu J, Wu X, Xie Z. Activation of RKIP binding ASC attenuates neuronal pyroptosis and brain injury via Caspase-1/GSDMD signaling pathway after intracerebral hemorrhage in mice. Transl Stroke Res. 2022;13(6):1037–54. https://doi.org/10.1007/s12975-022-01009-4.
27. Li R, Zhang X, Gu L, Yuan Y, Luo X, Shen W, Xie Z. CDGSH iron sulfur domain 2 over-expression alleviates neuronal ferroptosis and brain injury by inhibiting lipid peroxidation via AKT/mTOR pathway following intracerebral hemorrhage in mice. J Neurochem. 2023;165(3):426–44. https://doi.org/10.1111/jnc.15785.
28. Wu X, Fu S, Liu Y, Luo H, Li F, Wang Y, Gao M, Cheng Y, Xie Z. NDP-MSH binding melanocortin-1 receptor ameliorates neuroinflammation and BBB disruption through CREB/Nr4a1/NF-κB pathway after intracerebral hemorrhage in mice. J Neuroinflammation. 2019;16(1):192. https://doi.org/10.1186/s12974-019-1591-4.
29. Zeng J, Chen Y, Ding R, Feng L, Fu Z, Yang S, Deng X, Xie Z, Zheng S. Isoliquiritigenin alleviates early brain injury after experimental intracerebral hemorrhage via suppressing ROS- and/or NF-κB-mediated NLRP3 inflammasome activation by promoting Nrf2 antioxidant pathway. J Neuroinflammation. 2017;14(1):119. https://doi.org/10.1186/s12974-017-0895-5.
30. Huang D-D, Fan S-D, Chen X-Y, Yan X-L, Zhang X-Z, Ma B-W, Yu D-Y, Xiao W-Y, Zhuang C-L, Yu Z. Nrf2 deficiency exacerbates frailty and sarcopenia by impairing skeletal muscle mitochondrial biogenesis and dynamics in an age-dependent manner. Exp Gerontol. 2019;119:61–73. https://doi.org/10.1016/j.exger.2019.01.022.
31. Gu L, Sun M, Li R, Zhang X, Tao Y, Yuan Y, Luo X, Xie Z. Didymin suppresses microglia pyroptosis and neuroinflammation through the Asc/Caspase-1/GSDMD pathway following experimental intracerebral hemorrhage. Front Immunol. 2022;13:810582. https://doi.org/10.3389/fimmu.2022.810582.
32. Suzuki H. How to promote hemoglobin scavenging or clearance and detoxification in hemorrhagic stroke. Transl Stroke Res. 2023;14(5):625–7. https://doi.org/10.1007/s12975-022-01075-8.
33. Xia F, Keep RF, Ye F, Holste KG, Wan S, Xi G, Hua Y. The fate of erythrocytes after cerebral hemorrhage. Transl Stroke Res. 2022;13(5):655–64. https://doi.org/10.1007/s12975-021-00980-8.
34. Li X, Chen G. Mitochondrial-based therapeutic strategies for intracerebral hemorrhage. Transl Stroke Res. 2022;13(2):214–5. https://doi.org/10.1007/s12975-021-00966-6.
35. Nicholls DG, Budd SL. Mitochondria and neuronal survival. Physiol Rev. 2000;80(1):315–60. https://doi.org/10.1152/physrev.2000.80.1.315.
36. Cheng X-T, Huang N, Sheng Z-H. Programming axonal mitochondrial maintenance and bioenergetics in neurodegeneration and regeneration. Neuron. 2022;110(12):1899–923. https://doi.org/10.1016/j.neuron.2022.03.015.
37. Chen W, Guo C, Feng H, Chen Y. Mitochondria: novel mechanisms and therapeutic targets for secondary brain injury after intracerebral hemorrhage. Front Aging Neurosci. 2020;12:615451. https://doi.org/10.3389/fnagi.2020.615451.
38. Forrester SJ, Kikuchi DS, Hernandes MS, Xu Q, Griendling KK. Reactive oxygen species in metabolic and inflammatory signaling. Circ Res. 2018;122(6):877–902. https://doi.org/10.1161/CIRCRESAHA.117.311401.
39. Wang J, Zhou H. Mitochondrial quality control mechanisms as molecular targets in cardiac ischemia-reperfusion injury. Acta Pharm Sin B. 2020;10(10):1866–79. https://doi.org/10.1016/j.apsb.2020.03.004.
40. Muneoka S, Goto M, Nishimura T, Enomoto K, Kadoshima-Yamaoka K, Tomimori Y. G protein-coupled receptor 39 agonist improves concanavalin A-induced hepatitis in mice. Biol Pharm Bull. 2019;42(8):1415–8. https://doi.org/10.1248/bpb.b18-00982.
41. Xu Y, Wang M, Xie Y, Jiang Y, Liu M, Yu S, Wang B, Liu Q. Activation of GPR39 with the agonist TC-G 1008 ameliorates ox-LDL-induced attachment of monocytes to endothelial cells. Eur J Pharmacol. 2019;858:172451. https://doi.org/10.1016/j.ejphar.2019.172451.
42. Xu Y, Barnes AP, Alkayed NJ. Role of GPR39 in neurovascular homeostasis and disease. Int J Mol Sci. 2021;22(15). https://doi.org/10.3390/ijms22158200
43. Li J, Shi X, Chen Z, Xu J, Zhao R, Liu Y, Wen Y, Chen L. Aldehyde dehydrogenase 2 alleviates mitochondrial dysfunction by promoting PGC-1α-mediated biogenesis in acute kidney injury. Cell Death Dis. 2023;14(1):45. https://doi.org/10.1038/s41419-023-05557-x.
44. Sharma DR, Sunkaria A, Wani WY, Sharma RK, Verma D, Priyanka K, Bal A, Gill KD. Quercetin protects against aluminium induced oxidative stress and promotes mitochondrial biogenesis via activation of the PGC-1α signaling pathway. Neurotoxicology. 2015;51:116–37. https://doi.org/10.1016/j.neuro.2015.10.002.
45. Vekaria HJ, Hubbard WB, Scholpa NE, Spry ML, Gooch JL, Prince SJ, Schnellmann RG, Sullivan PG. Formoterol, a β2-adrenoreceptor

agonist, induces mitochondrial biogenesis and promotes cognitive recovery after traumatic brain injury. Neurobiol Dis. 2020;140:104866. https://doi.org/10.1016/j.nbd.2020.104866.
46. Zhang L, Tan X, Song F, Li D, Wu J, Gao S, Sun J, Liu D, Zhou Y, Mei W. Activation of G-protein-coupled receptor 39 reduces neuropathic pain in a rat model. Neural Regen Res. 2024;19(3):687–96. https://doi.org/10.4103/1673-5374.380905.
47. Jing W, Sun W, Zhang N, Zhao C, Yan X. The protective effects of the GPR39 agonist TC-G 1008 against TNF-α-induced inflammation in human fibroblast-like synoviocytes (FLSs). Eur J Pharmacol. 2019;865:172663. https://doi.org/10.1016/j.ejphar.2019.172663.
48. Shao L, Chen S, Ma L. Secondary brain injury by oxidative stress after cerebral hemorrhage: recent advances. Front Cell Neurosci. 2022;16:853589. https://doi.org/10.3389/fncel.2022.853589.
49. Chen S, Li L, Peng C, Bian C, Ocak PE, Zhang JH, Yang Y, Zhou D, Chen G, Luo Y. Targeting oxidative stress and inflammatory response for blood-brain barrier protection in intracerebral hemorrhage. Antioxid Redox Signal. 2022;37(1–3):115–34. https://doi.org/10.1089/ars.2021.0072.
50. Yang P, Feng Q, Meng L, Tang R, Jiang Y, Liu H, Si H, Li M. The mechanism underlying the TC-G 1008 rescue of reactive oxygen species (ROS)-induced osteoblast apoptosis by the upregulation of peroxiredoxin 1. Int J Biochem Cell Biol. 2022;151:106276. https://doi.org/10.1016/j.biocel.2022.106276.
51. Wang D, Wang Y, Zou X, Shi Y, Liu Q, Huyan T, Su J, Wang Q, Zhang F, Li X, et al. FOXO1 inhibition prevents renal ischemia-reperfusion injury via cAMP-response element binding protein/PPAR-γ coactivator-1α-mediated mitochondrial biogenesis. Br J Pharmacol. 2020;177(2):432–48. https://doi.org/10.1111/bph.14878.
52. Lee J, Kim C-H, Simon DK, Aminova LR, Andreyev AY, Kushnareva YE, Murphy AN, Lonze BE, Kim K-S, Ginty DD, et al. Mitochondrial cyclic AMP response element-binding protein (CREB) mediates mitochondrial gene expression and neuronal survival. J Biol Chem. 2005;280(49):40398–401. https://doi.org/10.1074/jbc.C500140200.
53. Zhao L-J, Zhang S-F. Activation of TGR5 promotes mitochondrial biogenesis in human aortic endothelial cells. Biochem Biophys Res Commun. 2018;500(4):952–7. https://doi.org/10.1016/j.bbrc.2018.04.210.
54. Yan J, Xu W, Lenahan C, Huang L, Wen J, Li G, Hu X, Zheng W, Zhang JH, Tang J. CCR5 Activation Promotes NLRP1-Dependent Neuronal Pyroptosis via CCR5/PKA/CREB Pathway After Intracerebral Hemorrhage. Stroke. 2021;52(12):4021–32. https://doi.org/10.1161/STROKEAHA.120.033285.

Publisher's Note Springer Nature remains neutral with regard to jurisdictional claims in published maps and institutional affiliations.

Springer Nature or its licensor (e.g. a society or other partner) holds exclusive rights to this article under a publishing agreement with the author(s) or other rightsholder(s); author self-archiving of the accepted manuscript version of this article is solely governed by the terms of such publishing agreement and applicable law.

Authors and Affiliations

Zhongyi Zhang[1] · Ye Yuan[1] · Xingyu Zhang[1] · Lingui Gu[2] · Yuguang Tang[1] · Yutong Zhao[1] · Jinyu Dai[1] · Yihao Tao[1] · Zongyi Xie[1]

✉ Yihao Tao
tyheva@cqmu.edu.cn

✉ Zongyi Xie
zyxie2008@cqmu.edu.cn

Zhongyi Zhang
2021110375@stu.cqmu.edu.cn

Ye Yuan
yunnicao@stu.cqmu.edu.cn

Xingyu Zhang
251233955@qq.com

Lingui Gu
gulingui1024@student.pumc.edu.cn

Yuguang Tang
2021120411@stu.cqmu.edu.cn

Yutong Zhao
2021150120@stu.cqmu.edu.cn

Jinyu Dai
2022110333@stu.cqmu.edu.cn

[1] Department of Neurosurgery, The Second Affiliated Hospital, Chongqing Medical University, Chongqing 400010, China

[2] Department of Neurosurgery, Center for Malignant Brain Tumors, National Glioma MDT Alliance, Peking Union Medical College Hospital, Chinese Academy of Medical Sciences and Peking Union Medical College, Beijing 100730, China